Size-resolved process understanding of stratospheric sulfate aerosol following the Pinatubo eruption

Allen Hu[1,*], Ziming Ke[2,*], Xiaohong Liu[1], Benjamin Wagman[3], Hunter Brown[3], Zheng Lu[1], Mingxuan Wu[4], Hailong Wang[4], Qi Tang[2], Diana Bull[3], and Kara Peterson[3], and Shaocheng Xie[2]

[1]Department of Atmospheric Sciences, Texas A&M, College Station TX, 77843, United States
[2]Lawrence Livermore National Laboratory, Livermore CA, 94550, United States
[3]Sandia National Laboratories, Albuquerque NM, 87185, United States
[4]Pacific Northwest National Laboratory, Richland WA, 99352, United States

* These authors contributed equally to this work.

Correspondence to: Xiaohong Liu (xiaohong.liu@tamu.edu)

Abstract. Stratospheric sulfate aerosol produced by volcanic eruptions plays important roles in atmospheric chemistry and the global radiative balance of the atmosphere. The simulation of stratospheric sulfate concentrations and optical properties is highly dependent on the chemistry scheme and microphysical treatment. In this work, we implemented a sophisticated gas-phase chemistry scheme (full chemistry, FC) and a 5-mode version of the Modal Aerosol Module with Prognostic Stratospheric Aerosol (MAM5-PSA) for the interactive treatment of stratospheric sulfate aerosol in the Department of Energy's Energy Exascale Earth System Model version 2 (E3SMv2) model to better simulate the chemistry-aerosol feedback following the Pinatubo eruption, and to compare it against a simulation using simplified chemistry (SC) and the default 4-mode version of the Modal Aerosol Module (MAM4). MAM5-PSA experiments were found to better capture the stratospheric sulfate burden from the eruption of the volcano to the end of 1992 as compared to the High-resolution Infrared Sounder (HIRS) observations, and the formation of sulfate in MAM5-PSA with FC (with an additional OH replenishment reaction) was significantly faster than in MAM4 with FC . Analyses of microphysical processes indicate that more sulfate aerosol mass was generated in total in FC experiments than in SC experiments. MAM5-PSA performs better than MAM4 in simulation of aerosol optical depth (AOD); AOD anomalies from the MAM5-PSA experiment have better agreement with observations. The simulated largest changes in global mean net radiative flux at the top of the atmosphere following the eruption were about -3 W/m^2 in MAM5-PSA experiments and roughly -1.5 W/m^2 in MAM4 experiments.

1 Introduction

Explosive volcanic eruptions can inject material and gas-phase aerosol precursors into the stratosphere, affecting atmospheric chemistry and radiation and often leading to significant global-scale cooling at the surface (Yang and Schlesinger, 2002; Parker et al., 1996). Many major volcanic eruptions have been associated with dramatic drops in temperature, famine and even the absence of a summer season (Robock, 2000), though Mt. Pinatubo was the first major eruption to be observed with modern instruments. Background stratospheric aerosol during volcanically quiescent periods have optical depths of less than 0.01 and a total stratospheric burden of roughly 0.1 Tg (Sheng et al., 2015; Deshler, 2008), and mainly consist of sulfate formed through the oxidation of sulfur dioxide (SO_2) and carbonyl sulfide (OCS) emitted at the Earth's surface (Sheng et al., 2015). These background aerosols are often overshadowed by sulfate aerosols produced by volcanic eruptions, which are formed from the oxidation of SO_2 into sulfuric acid and subsequent nucleation and condensation to form sulfate aerosol in the stratosphere (Mills et al., 2016). These particles have a lifespan on the order of years, so it is rare for the stratosphere to be unperturbed by volcanic emissions (Seinfeld and Pandis, 2016). Eventually, these stratospheric aerosols are removed by entering the troposphere through sedimentation processes and cross tropopause air mixing (Kremser et al., 2016).

The eruption of interest in this study is the Mt. Pinatubo eruption on June 15, 1991. It was one of the most powerful volcanic eruptions in recent decades and occurred after the onset of various modern observation techniques. The amount of SO_2 injected into the atmosphere was likely in the range of 15 to 18 Tg (Carn, 2022; Neely Iii, 2016; Aubry et al., 2021). A significant cooling of approximately 0.5 degree at the Earth's surface was observed afterwards due to

the strong scattering of solar shortwave radiation by sulfate aerosol (Parker et al., 1996). In recent years interest in geoengineering as a countermeasure against the effects of climate change has been growing (Crutzen, 2006), with a concept that is analogous to that of a volcanic eruption; sulfate aerosol, formed from SO_2 that is deliberately injected into the stratosphere, could lead to significant temperature decreases at the Earth's surface. It is therefore essential to examine volcanic eruptions for better modeling of future eruptions and better understanding of the effects of geoengineering.

~~Previous studies have shown that the impacts of volcanic aerosol injections on climate are dependent on the latitude, aerosol type, and season of the injection of volcanic aerosols. Tilmes et al. (2017) examined the aerosol loadings and climate responses associated with hypothetical SO_2 injections at different heights and latitudes using the Whole Atmosphere Community Climate Model (WACCM), finding that continuous high-altitude injections (above the equator, 15°S and 15°N, 30°S and 30°N respectively) at 5 km above the tropopause produced 50% higher aerosol burdens than equivalent injections at 1 km above the tropopause due to a longer sedimentation path, although low-altitude injections transported more efficiently from the tropics to the midlatitudes, leading to similar temperature decreases (Tilmes et al., 2017). Injections at 15° N and 15° S were found to transport more efficiently to middle and high latitudes and produce higher global mean AOD than injections at the equator due to the influence from the Brewer-Dobson circulation and the polar vortex (Tilmes et al., 2017). Injections at the 30° and 50° latitudes do not efficiently transport towards the tropics. Laakso et al. (2017) investigated the climatic effects of seasonally varying sulfate injections in the Max Planck Institute's Earth System Model (MPI-ESM). They found that, relative to the experiment with stationary injections above the equator, equivalent injections at the latitudinal position of the maximum solar radiation (for example, at 20-40°N in April and at 20-40°S in October) would lead to 15% stronger radiative forcing outside 20°S-20°N but 27% weaker forcing within this area.~~

Numerous previous studies have examined volcanic effects on climate and possible influencing factors such as the location and timing of the eruption and total emissions. Using statistical emulation of output of the UK Met Office Unified Model coupled with the UK Chemistry and aerosol scheme (UK-UMCA), Marshall et al. (2019) found that for large SO_2 emissions of 10 to 100 Tg, the e-folding decay time for the global sulfate aerosol burden is most dependent on the latitude of the eruption, while the integrated global mean stratospheric AOD and net radiative forcing is most dependent on the total mass of the SO_2 emissions. Zhuo et al. (2024) used the Whole Atmosphere Community Climate Model Version 6 (WACCM6) to simulate volcanic eruptions on a similar scale to Pinatubo from Central America and Iceland under different ENSO initial states, finding that initial atmospheric conditions control the meridional transport of sulfur and halogens in the first month after the eruptions as well as further modulating the latitudinal distribution of sulfate aerosols, halogens, volcanic forcing and impacts. Toohey et al. (2019) analyzed ice-core-derived volcanic stratospheric sulfur injections and Northern Hemisphere summer temperature reconstructions from tree rings, finding that in proportion to their estimated stratospheric sulfur injection, extratropical explosive eruptions since 750 CE have produced stronger hemispheric cooling than tropical eruptions; stratospheric aerosol

simulations with the MAECHAM5-HAM model suggested that this was due to the enhanced radiative impact associated with the relative confinement of aerosol to a single hemisphere.

Previous studies regarding stratospheric aerosols utilize different methods to simulate aerosol properties and microphysics. The simplest and most direct approach is to prescribe stratospheric aerosol properties or burdens using climatology derived from observations. For example, Zhuo et al. (2021) produced volcanic forcing using the Easy Volcanic Aerosol (EVA) module, which directly generated stratospheric aerosol optical properties for the given volcanic emissions. More sophisticated methods primarily include bulk schemes, modal schemes, and sectional schemes (Liu, 2023). Bulk schemes are the simplest, where aerosols species are not divided into bins or modes, and properties such as size distribution are prescribed. CNRM-ESM2-1 (an Earth system model developed by the Centre National de Recherches Météorologiques) – one of the models used in Tilmes et al. (2022) for a model intercomparison project for geoengineering – prescribed stratospheric aerosol size distributions with no interactive aerosol microphysics. Gao et al. (2023) used the GFDL Earth System Model version 4.1 (GFDL ESM4.1) to prognostically simulate stratospheric sulfate aerosol concentrations for volcanic eruptions but aerosol size was prescribed, with a sulfate dry effective radius of 0.166 μm, 0.25 μm, 0.4 μm or 1 μm in different sensitivity experiments. Modal schemes typically divide the aerosol population according to the modes conventionally used to describe aerosol size distributions (i.e., Aitken mode, accumulation mode, coarse mode, and nucleation mode in some schemes), with each mode having its own prescribed standard deviations of ~~log-normal~~lognormal distributions while mass and number concentrations of aerosols in each mode are predicted (Mills et al., 2016; Visioni et al., 2023). Mills et al. (2016) used WACCM's three mode version of the Modal Aerosol Module (MAM3) to simulate the Pinatubo eruption by altering the parameters (e.g., standard deviation) of the coarse mode, but in doing so also influenced the simulation of unrelated coarse mode aerosols such as sea salt and dust, as the aerosols in each mode are treated as internal mixtures rather than being separated by species. Brown et al. (2024) simulated the Pinatubo eruption in E3SMv2 using a four mode version MAM (MAM4), with modifications to the default MAM4 used in E3SMv2. Bin schemes (or sectional schemes) divide aerosols into more categories than modal schemes, providing greater resolution with the drawback of additional computational cost. Vattioni et al. (2019) used a sectional aerosol module which was capable of handling aerosols in 40 different size bins to better represent accumulation-mode H_2SO_4 of stratospheric aerosol and their direct injection into the atmosphere as opposed to injections of SO_2. Laakso et al. (2022) simulated sulfur injection in the stratosphere using the Sectional Aerosol module for Large Scale Applications (SALSA) which utilized 10 size bins.

Recent studies of volcanic eruptions or stratospheric sulfate related to geoengineering have utilized different approaches with regards to stratospheric chemistry. Zhuo et al. (2021) omitted chemistry of sulfate formation entirely, with SO_2 emissions directly being converted into aerosol optical properties through empirical calculations. Some studies used a simplified chemistry scheme. In the SALSA1 scheme introduced in Kokkola et al. (2008) and implemented in Bergman et al. (2012), prescribed hydroxyl radical (OH) concentrations were used for stratospheric chemistry. Kleinschmitt et al. (2018) used a prescribed SO_2 to H_2SO_4 conversion rate in the Sectional Stratospheric Sulfate Aerosol (S3A) module to simulate SO_2 injections. Kleinschmitt et al. (2017) reported a doubling of SO_2

lifetime in the stratosphere when OH is prognostically calculated for major injections of SO_2, such as the Pinatubo eruption, but did not quantitatively compare scenarios with OH prescribed or not prescribed. Studies that used WACCM, such as Mills et al. (2016) and Visioni et al. (2019), considered the key chemical reactions within the stratosphere with a prognostic treatment of OH for the oxidation of SO_2 to form sulfate aerosol.

This paper builds upon the work of Mills et al. (2016) and Brown et al. (2024) by adding a unique stratospheric sulfate coarse mode and by considering the full chemistry in E3SM, to simulate the burden, AOD, and radiative effect of volcanic aerosols. Brown et al. (2024) also simulated the Pinatubo eruption using E3SMv2, the same version of the earth system model as this study. Their prognostic aerosol simulations use the model's default "simple" chemistry, the same as our SC experiments. One of their experiments, E3SMv2-PA, used the default MAM4 (i.e., nearly identical to our MAM4SC experiment). Their other prognostic aerosol experiment, E3SMv2-SPA, used a revised MAM4, which treated dust, sea salt and stratospheric sulfate using the same coarse mode parameters, such as size range and geometric standard deviation, specifically chosen to best represent stratospheric sulfate properties, resulting in erroneous coarse mode dust and sea salt aerosol concentrations. To avoid these problems, this study establishes a fifth aerosol mode (MAM5-PSA), the stratospheric coarse mode, to specifically handle stratospheric sulfate. The coarse mode remains the same as the original MAM4 to handle dust and sea salt. ~~Brown et al. (2024)~~OOur aim is to (1) examine the differences in simulated sulfate aerosol burden after the Pinatubo eruption with and without the addition of the stratospheric coarse mode to MAM~~changes in MAM~~; (2) examine the differences in sulfate between using E3SM's default "simple" chemistry and a sophisticated "full" chemistry treatment; and (3) quantify the microphysical processes involved in sulfate chemistry and modal aerosol. It is worth noting that changes in stratospheric ozone following volcanic eruptions play a significant role in both stratospheric chemistry and the impacts on temperature, but it is not the focus for this paper.

The model set-up, including aerosol module, chemistry settings, emissions, nudging, and observational data are described in Section 2. Section 3.1 presents the simulated spatial distribution and total burden of stratospheric sulfate aerosols following the Pinatubo eruption, and Section 3.2 engages in process analyses of the sulfate aerosols and discusses their growth processes in the different experiments. Section 4 presents the conclusion of our research.

2 Methodology

2.1 Model overview

The model utilized in this study is E3SMv2, which runs roughly twice as fast relative to E3SMv1. The model contains further changes to the dynamical core, the dynamical grid and parameterization column grid, and atmospherics physics and chemistry (Golaz et al., 2022). By default, E3SMv2 treats aerosols through an enhanced version of MAM4 with all aerosol types appearing in the coarse mode (Liu et al., 2016), in which the four lognormal size modes represent the Aitken mode, accumulation mode, coarse mode and primary carbon mode respectively (the primary carbon mode is not directly relevant for our study of stratospheric sulfate aerosol). The model also simulates aerosol microphysical

processes relevant to stratospheric sulfate, including condensation, nucleation, coagulation, and water uptake. The experiments are run under the "ne30pg2" resolution, with a grid spacing of approximately 110 km for dynamics and about 165 km for physics. Vertically, it has 72 layers of varying thicknesses, with the top at roughly 60 km altitude (Golaz et al., 2022). The emissions and wet and dry removal of aerosols were described in Wang et al. (2020).

~~In E3SMv2 MAM4, the coarse mode was primarily intended for coarse sea salt and dust, as well as other aerosol species resuspended from raindrop evaporation, with a geometric standard deviation of 1.8, and stratospheric sulfate aerosol cannot enter the coarse mode through renaming (a process in which aerosol particles that grow larger than a given threshold via condensation and coagulation are transferred from one mode to another, rather than staying in the original mode and instead increasing in number to conserve mass) (Liu et al., 2016). In this study, we utilize a new five-mode version of the Modal Aerosol Module with prognostic stratospheric aerosol (MAM5-PSA) to represent aerosol processes. MAM5-PSA is similar to MAM4 but has a fifth mode added to specifically represent stratospheric coarse-mode sulfate aerosol. Renaming is allowed from the accumulation mode into stratospheric coarse mode in MAM5-PSA. This fifth mode has a smaller geometric standard deviation (1.2) for aerosol size aiming to more accurately reflect the gravitational settling velocity of volcanic sulfate aerosol from the atmosphere (Mills et al., 2016). The stratosphere coarse mode is separate from the original coarse mode in MAM4 so that the changes to better represent volcanic aerosol properties do not affect other coarse mode aerosols such as dust and sea salt.~~

In E3SMv2 MAM4, the coarse mode was primarily intended for coarse sea salt and dust, as well as other aerosol species resuspended from raindrop evaporation, with a geometric standard deviation of 1.8, and stratospheric sulfate aerosol cannot enter the coarse mode through renaming. Renaming is a process in which aerosol particles that grow larger than a given threshold via condensation and coagulation are transferred from one mode to another. To avoid these problems, this study establishes a fifth aerosol mode (MAM5-PSA), the stratospheric coarse mode, to specifically handle stratospheric sulfate. The coarse mode remains the same as the original MAM4 to handle dust and sea salt. The newly added stratospheric coarse mode follows the same size parameters as the revised coarse mode in Mills et al. (2016) and Brown et al. (2024) to better reflect stratospheric sulfate lifespans, but handles stratospheric sulfate separately from coarse mode sea salt and dust. A portion of sufficiently large accumulation mode sulfate aerosols are permitted to transfer to the stratospheric coarse mode through renaming. It should be noted that the upper limit for the accumulation mode size range is larger than the lower limit for the stratospheric coarse mode size range, leading to potential size overlaps between the two modes' aerosol populations.

~~This is an improvement upon Mills et al. (2016) and Brown et al. (2024) in which volcanic sulfate aerosols were not separated from other coarse mode aerosols.~~

To understand the mechanisms of simulated sulfate aerosol in MAM5-PSA, we carry out process analyses for (a) NUCL (nucleation), (b) COAG (coagulation) and (c) RNMaa (renaming from Aitken mode to accumulation mode), and (d) RNMasc (renaming from accumulation mode to stratospheric coarse mode) (Fig. 1(a)). Condensation processes for each of the modes have also been included, with the positive values representing the transition of mass from the gaseous phase to the aerosol. Each of these processes have their rules and requirements within MAM:

- NUCL, or nucleation, is responsible for the formation of aerosols starting from the Aitken mode (nucleation mode aerosols are not represented in MAM).
- COAG, or coagulation, represents two smaller particles colliding to form a larger particle. MAM considers the intramodal and intermodal coagulation of the Aitken, accumulation and primary carbon modes. Intramodal coagulation reduces the number of the mode but leaves the mass unchanged. Intermodal coagulation between these modes and the coarse mode is not considered in MAM.
- AitkenCond, or condensation in the Aitken mode, leading to aerosol mass increase in the Aitken mode population. No matter how much mass is gained from condensation, the aerosols cannot grow into the accumulation mode directly, it MUST undergo renaming.
- AccumCond and StratoCoarseCond, condensation for the accumulation mode and stratospheric coarse mode, work similarly.
- RNMaa, or renaming from the Aitken to accumulation mode. Periodically, the size of the Aitken mode aerosol population is checked. If a specified threshold is reached (due to mass increase from the condensation and coagulation processes), then aerosol number and mass are transferred from the Aitken mode to the accumulation mode.
- RNMasc, renaming from the accumulation mode to stratospheric coarse mode. No other microphysical process is allowed to produce stratospheric coarse mode sulfates, so this is their only source.

Formatted: Indent: Left: 0.81", No bullets or numbering

We also improve the E3SMv2 to output these tendencies in 2D after the 3D tendencies are vertically integrated.

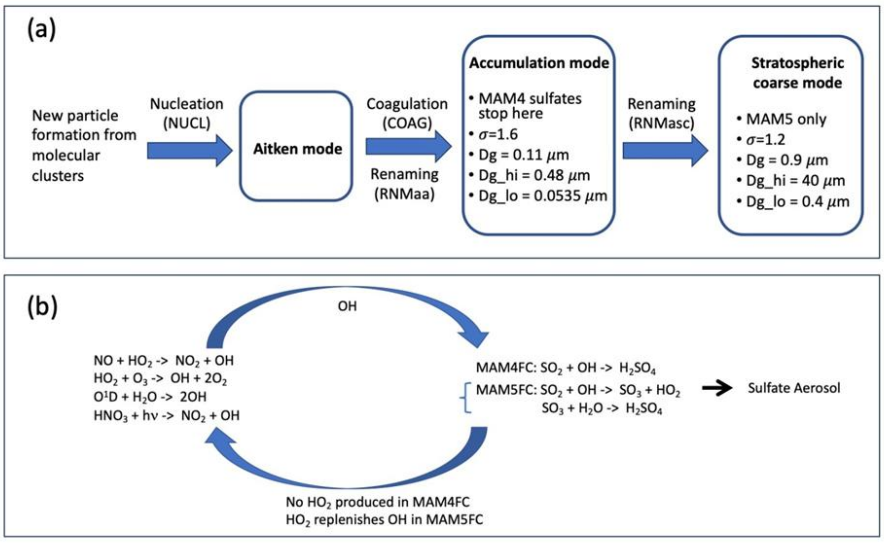

Figure 1: (a) Flowchart depicting the aerosol modes and analyzed microphysical processes for the formation of stratospheric sulfate in our experiments. The parameters for the lognormal size distribution of the accumulation mode and stratospheric coarse mode are shown. σ represents the geometric standard deviation of aerosol number concentration (a smaller standard deviation corresponds to a longer atmospheric lifespan).~~, and Dg, Dg_hi, and Dg_lo represent the geometric dry mean diameter and its upper and lower limits, respectively. Dg values are not static within the model and the values given can be seen as a reference value.~~ Renaming is a process within E3SM where aerosols that grow sufficiently large can transfer from one mode to another. (b) Chart that depicts the differences in the full chemistry (FC) between MAM4 and MAM5-PSA. In MAM4FC, the oxidation of SO_2 by OH radicals directly produces H_2SO_4 with no byproducts. In MAM5FC, this reaction instead produces HO_2 and SO_3. SO_3 eventually converts into sulfuric acid, while HO_2 is crucial in the replenishment of OH concentrations.

Note that the geometric dry mean diameter (Dg) values are prognostically calculated and can become larger or smaller than the initial prescribed Dg value given in Fig. 1(a) depending on microphysical processes. Dg_hi and Dg_lo are the upper and lower limits for the geometric dry mean diameter. These values are comparable to those used in Mills et al. (2016) so as to maintain parity.

2.2 Chemical mechanisms

By default, E3SMv2 uses a simplified set of chemical species and reactions (hereafter referred to as "simple chemistry" or "SC") that omits many less important species and reactions in order to save computational costs. Tracer species in the model have prognostically evolving concentrations and include H_2O_2, dimethyl sulfide (DMS), sulfuric acid (H_2SO_4), SO_2, secondary organic aerosol precursor gases, and aerosols. Prescribed species such as oxygen, ozone, OH, and HO_2 have fixed, predetermined concentrations. Photolysis is restricted to H_2O_2 (and is simplified to produce no product); beyond that, there are only six other reactions:

$$DMS + OH \rightarrow SO_2 \quad \text{(R1)}$$

$$DMS + OH \rightarrow 0.5SO_2 + 0.5HO_2 \quad \text{(R2)}$$

$$DMS + NO_3 \rightarrow SO_2 + HNO_3 \quad \text{(R3)}$$

$$HO_2 + HO_2 \rightarrow H_2O_2 \quad \text{(R4)}$$

$$H_2O_2 + OH \rightarrow H_2O + HO_2 \quad \text{(R5)}$$

$$SO_2 + OH \rightarrow H_2SO_4 \quad \text{(R6)}$$

To better simulate the stratospheric chemistry following a volcanic eruption – albeit at greater computational cost (roughly twice that of SC) – a "full chemistry" (FC) setup is added through replacing the chemistry preprocessor. It is similar to the Model of Ozone and Related chemical Tracers (MOZART) chemistry scheme (Emmons et al., 2010) used in WACCM (Mills et al. (2016); the original work for E3SM is based on Wu et al. (2022), with some relevant stratospheric gas phase reactions added in. This scheme can handle many organic compounds that are ignored in the simple chemistry, containing 16 photolysis reactions and 41 stratospheric reactions that influence the concentrations of many radical species in the stratosphere. Most importantly, OH radicals (as well as other oxidants) are prognostically calculated rather than using prescribed values. This allows the model to represent the localized depletion of these species due to the injection of large amounts of SO_2, bottlenecking aerosol formation rates.

With the definitions of SC and FC described above, we consider combinations of MAM4SC, MAM4FC, MAM5SC, and MAM5FC in this study (Table 1). One further change is made for MAM5FC: for the oxidation of SO_2 to form sulfuric acid, the reaction in MAM4FC is $SO_2 + OH \rightarrow H_2SO_4$, whereas the reactions in MAM5FC are

$$SO_2 + OH \rightarrow SO_3 + HO_2 \quad \text{(R7)}$$

$$SO_3 + H_2O \rightarrow H_2SO_4 \quad \text{(R8)}$$

HO_2 participates in the replenishment of OH radicals in the stratosphere in MAM5FC, a process that is significantly slower in MAM4FC due to the above reaction not producing HO_2 (Fig. 1(b)).

2.3 Experimental set-up

In order to examine the differences between MAM4/MAM5-PSA and simple/full chemistry in E3SMv2's simulation of Pinatubo, one experiment is performed for each permutation. Coupled Model Intercomparison Project Phase 6 (CMIP6) Diagnosis, Evaluation and Characterization of Klima (DECK) emissions files are used with the exception of volcanic emissions, which consists of VolcanEESM emissions regridded and merged into CMIP6 SO_2 emissions (Brown et al., 2024). Pinatubo eruptions are assumed to have occurred on June 15 1991, with 10 Tg of SO_2 evenly emitted between 18 and 20 km altitude, identical to Mills et al. (2016). This is smaller than the observed SO_2 emissions because E3SM does not consider volcanic ash or water vapor emissions nor consequent ice sequestration of SO_2 and fallout of ash and ice particles. Sea ice and sea surface temperatures are prescribed according to CMIP6 DECK datasets. Each simulation starts from January 1, 1991, with more than six months as spin up time. Only the meridional and zonal winds were nudged to MERRA-2 reanalysis leaving the temperature and humidity to dynamically respond.

Formatted: Subscript

Table 1: List of numerical simulations.

Experiment name	Aerosol module	Chemistry
MAM4SC	MAM4	Simple chemistry
MAM4FC	MAM4	Full chemistry
MAM5SC	MAM5-PSA	Simple chemistry
MAM5FC	MAM5-PSA	Full chemistry (with alterations)

2.4 Observational data

AVHRR monthly observations of AOD for the years of 1989-1993 were used for model evaluation. Observed AOD values at 600 nm were downloaded from https://www.ncei.noaa.gov/data/avhrr-aerosol-optical-thickness/access (last access: June 5 2024) (Zhao, 2022). The wavelength of observation is different from E3SMv2 which outputs AOD at 550 nm wavelength, but the discrepancy caused by the difference in wavelength can be considered negligible. The website provides retrieved monthly AOD with a spatial resolution of 0.1°×0.1°, calculated using AVHRR's daily orbital observation of top-of-atmosphere reflectance over the oceans. E3SM output AOD that is used to compare with AVHRR results is masked according to the pixels that were successfully observed by AVHRR and regridded to be

the same resolution. The Global Space-based Stratospheric Aerosol Climatology (GloSSAC) is a global and gap-free data set of zonally averaged optical properties of stratospheric aerosols (focused on aerosol extinction coefficient at 525 and 1020 nm) from 1976–2018 (Thomason et al., 2018). Here, we use the updated version 2 from Kovilakam et al. (2020). Sulfate burdens derived from HIRS observations according to Baran and Foot (1994) were used for model comparison. Data from the balloon-borne University of Wyoming optical particle counters (WOPC) (Deshler et al., 1993; Deshler et al., 2003) is converted from the original particle number size distributions to particle volume size distributions for comparisons with model outputs.

3 Results

3.1 Simulated concentrations of stratospheric sulfate

Figure 2 presents the simulated horizontal distributions of sulfate aerosol concentrations at 53 hPa at 3, 9 and 15 days after the eruption of Pinatubo respectively for the four experiments. The overall distribution pattern is similar between all four experiments, with sulfate aerosol spreading westwards from Mt. Pinatubo in the Philippines following the eruption because of the Quasi-Biennial Oscillation. After 3 days, the sulfate reaches India; after 9 days, it passes over Africa and reaches the eastern coast of the Atlantic Ocean; after 15 days, it reaches Central America. Within this time period, northward and southward transport is both relatively weak, and the sulfate mostly remains between 30 °S and 30 °N (excluding background sulfates present prior to the eruption).

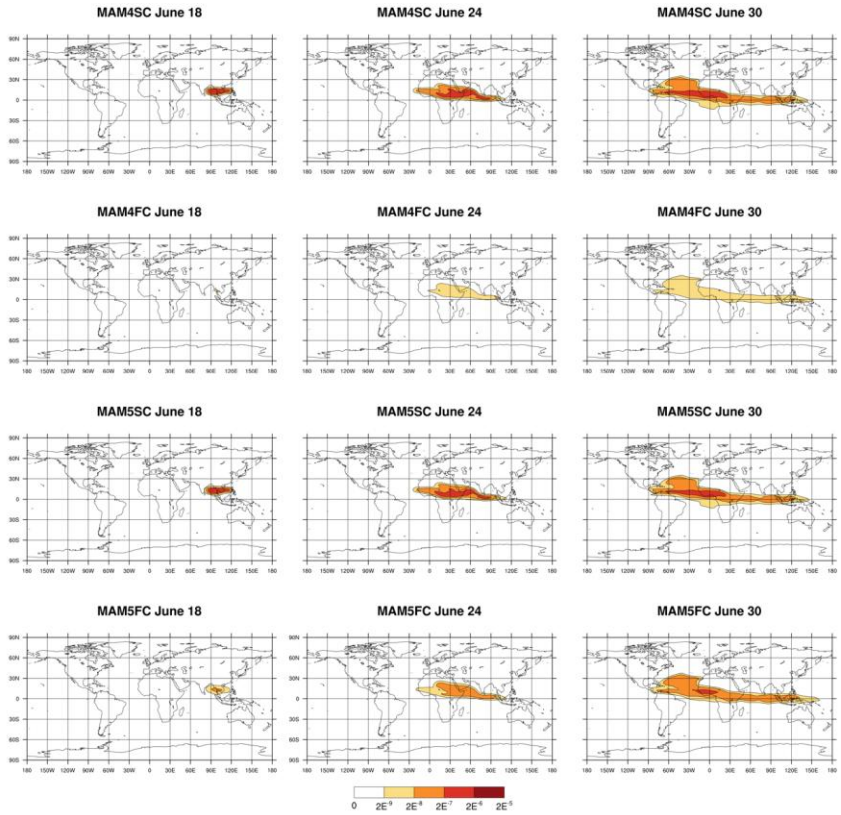

Figure 2: Simulated distributions of sulfate aerosol concentrations (kg/kg) at 53 hPa for days 3, 9 and 15 after the eruption of Pinatubo, respectively, for experiments MAM4SC (first row), MAM4FC (second row), MAM5SC (third row), and MAM5FC (bottom row).

For both MAM4 and MAM5-PSA simulations, sulfate concentrations are generally higher in SC than in FC. In these experiments, sulfate formation is not hindered by a lack of OH because OH concentration is prescribed and not depleted. On June 18, 3 days after the eruption, there is a substantial difference in sulfate concentrations near the origin of the plume. In MAM4SC and MAM5SC, the concentrations reach above 10^{-6} kg/kg. There is no replenishment mechanism for OH radical in MAM4FC, hindering sulfate formation, so the peak value in MAM4FC is below 10^{-8} kg/kg. In MAM5FC, OH can be depleted but a replenishment mechanism is also present, and the highest concentration is between 10^{-8} kg/kg and 10^{-7} kg/kg. These differences between SC and FC weaken over time as the plume spreads and encounters more OH to participate in the oxidation of SO_2 in FC. On June 30, the peak concentration in MAM4FC is between 10^{-8} and 10^{-7} kg/kg, while in the other three experiments it is between 10^{-7} and 10^{-6} kg/kg.

Figure 3 depicts the vertical profiles of sulfate concentrations for the Aitken and accumulation modes (or the sum of accumulation and stratospheric coarse modes for MAM5-PSA, as MAM4 cannot rename accumulation mode into coarse mode) in each of the four experiments. In all four experiments, the initial sulfate burden before July consists of mostly Aitken mode aerosols with peak concentrations on the order of 10^{-9} kg/kg. Sulfate aerosol either leaves the Aitken mode or is removed from the stratosphere within the span of several weeks in SC experiments, while sulfate persists past October in FC runs. Soon after July 1991, accumulation mode sulfate in MAM4 and accumulation mode plus stratospheric coarse mode sulfate in MAM5-PSA become dominant until they diminish back to background levels, with peak concentrations on the scale of 10^{-7} kg/kg.

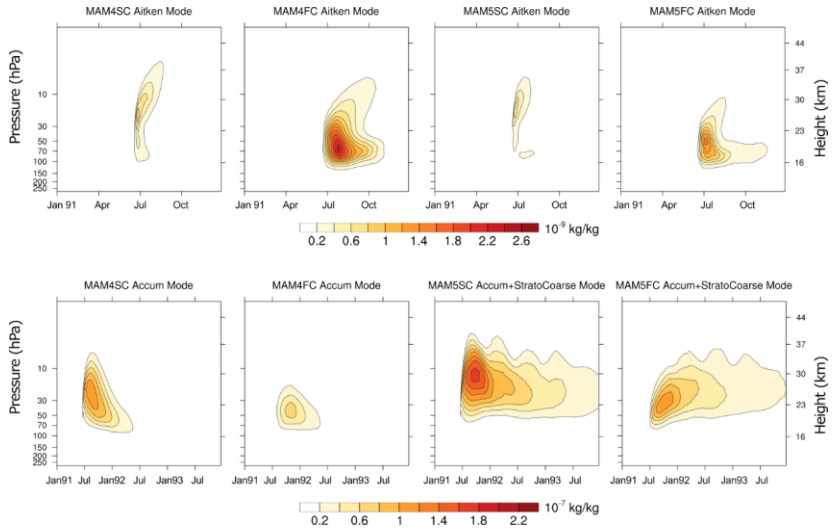

Figure 3: Vertical profiles of sulfate concentrations in the four experiments. The plots are divided by modes (Aitken mode in top panel with units of 10^{-9} kg/kg, accumulation mode or the sum of accumulation mode and stratospheric coarse mode for MAM5-PSA in bottom panel with units of 10^{-7} kg/kg). The plots for the Aitken mode aerosols span the year 1991 as the lifetime of the aerosols are within several months. The plots for the accumulation mode and stratospheric coarse mode aerosols span the years 1991 to 1993. The concentrations are averaged across longitude and latitude within the 30°S to 30°N band to remove interfering signals. Note that the top and bottom panels span different time periods.

There are significant differences in concentrations and locations of sulfate between SC and FC. In the SC experiments, both the earlier Aitken mode sulfate and the later accumulation and stratospheric coarse mode sulfate remain at a higher altitude than the corresponding FC experiments. The highest concentrations occur between 10 and 30 hPa altitudes for SC, and between 30 and 70 hPa altitudes for FC, which may be explained by the higher SO_2 concentrations at 30-70 hPa in FC relative to SC, the smaller negative difference in OH concentrations at 30-70 hPa in FC relative to SC, and the higher specific humidity at 30-70 hPa in FC compared to SC (Supplementary Figs. 1-4). For this same reason, the Aitken mode in FC generally has higher concentrations than SC after the eruption (up to 2.6×10^{-9} kg/kg in FC compared to less than 1.0×10^{-9} kg/kg in SC) in both the MAM4 and MAM5-PSA simulations. For the accumulation

and stratospheric coarse modes, SC generally has higher concentration than FC several weeks after the eruption (up to 1.0×10^{-7} kg/kg and 1.6×10^{-7} kg/kg for MAM4SC and MAM5SC respectively compared to less than 1.0×10^{-7} kg/kg in FC).

The main differences between MAM4 and MAM5-PSA are: (1) the inability of sulfate to progress past the accumulation mode in MAM4, and (2) the relatively short lifespan of the accumulation mode aerosols in MAM4 compared to the stratospheric coarse mode aerosols in MAM5-PSA. The shorter lifespan is a result of the MAM5-PSA's stratospheric coarse mode aerosols actually being smaller than MAM4's accumulation mode aerosols. Renaming from the accumulation mode to the stratospheric coarse mode in MAM5-PSA begins before the accumulation mode particles reach the maximum allowed size, which is easily reached in MAM4.. The stratospheric coarse mode also has a reduced geometric standard deviation of ~~the stratospheric coarse mode (~~1.2~~,~~ versus 1.6 for MAM4's accumulation mode~~ (,~~ as described in Fig. 1~~).~~. A smaller geometric standard deviation for stratospheric coarse mode in MAM5-PSA means that there are fewer super-coarse aerosols within the population. As super-coarse aerosols sediment more quickly, a smaller geometric standard deviation (1.2) leads to a longer lifespan for sulfate. In MAM4, constraining sulfate to the accumulation mode leads to aerosols, as well as the larger geometric standard deviation leads to a significant number of aerosols being super-coarse and quickly removed. Therefore, sulfate concentrations return to background level after roughly one year in MAM4 (as was also seen in E3SMv2-PA in Brown et al. (2024)) but this takes multiple years in MAM5-PSA.

3.2 Simulated burdens of stratospheric sulfate

Figure 4(a) shows the time series of the simulated stratospheric burden of sulfate between 80° S and 80° N, as well as the HIRS monthly observational data for stratospheric sulfate burden for the same latitude bands taken from Baran and Foot (1994). Note that the stratospheric burden derived from HIRS data assumes that the mean stratospheric temperature is 210K, which is increasingly inaccurate with more distance from the tropics. Following the eruption of Mt. Pinatubo on June 15, 1991, sulfate burdens in all four model experiments rise rapidly, reach their peak value in November 1991, then begin to diminish over time. MAM4SC, MAM5SC and MAM5FC have about the same peak sulfate burden of about 5.5 Tg, occurring at roughly the same time in November 1991. The rate of increase for the sulfate burden, as well as the eventual peak sulfate burden, is the lowest in MAM4FC (about 4.8 Tg sulfur on November 30, 1991) due to OH concentrations in the atmosphere being depleted by the extremely large amount of SO_2 produced by the eruption and being unable to replenish quickly. Starting in January 1992, the stratospheric burdens in MAM4 drop off more quickly compared to MAM5-PSA ~~due to the reduced geometric standard deviation in MAM5-PSA's stratospheric coarse mode, so MAM4's burden drops off excessively quickly compared to the HIRS observation whereas~~ and MAM5FC agrees closely with HIRS until the end of 1992. In MAM4, sulfate in the accumulation mode grows until it reaches its maximum allowed geometric dry mean diameter of 0.48 microns (the Dg_hi value for the accumulation mode). Under such situations, the sulfate aerosol population increases in number (and therefore mass), but the size cannot increase any further. In MAM5-PSA, renaming is permitted, and the transfer

from the accumulation mode to the stratospheric coarse mode begins when the geometric dry mean diameter is 0.40 microns (i.e. the Dg_lo value for the stratospheric coarse mode). Upon transfer to the stratospheric coarse mode, certain aerosol growth processes such as coagulation cease (as it is only allowed for the Aitken and accumulation modes in MAM), so the stratospheric coarse mode sulfates in MAM5-PSA tend to grow no larger in size, and the geometric dry mean diameter remains around 0.40 microns. In addition, ~~T~~the reduced geometric standard deviation of MAM5-PSA's stratospheric coarse mode (1.2) relative to MAM4's accumulation mode (1.6) also corresponds to a smaller proportion of ~~extremely large~~super-coarse aerosols that are removed more quickly from the stratosphere, due to the settling velocity being roughly proportional to the second power of the aerosol diameter (Seinfeld and Pandis, 2016). These two reasons are responsible for the sulfate having a longer lifespan in MAM5-PSA than MAM4. The burden in MAM5-PSA continues to decrease almost linearly in the following years but does not return to background levels until 1995 (not pictured). For both MAM4 and MAM5-PSA, the full chemistry experiments have stratospheric sulfate burdens that decline more quickly after reaching peak values in November 1991 than the corresponding simple chemistry experiment.

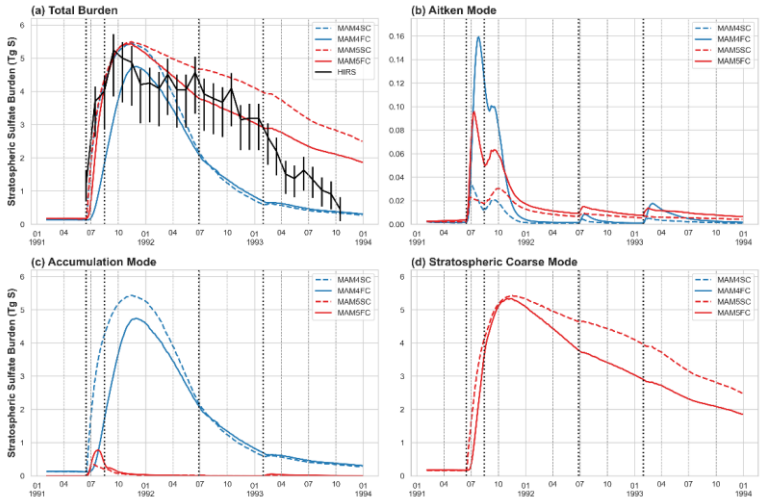

Figure 4: (a) Comparisons of simulated stratospheric sulfate burdens (Tg S) between 80° S and 80° N from the four experiments with HIRS observations for years of 1991-1995. Black line depicts the estimates made from HIRS data in Baran and Foot (1994), with the black bars representing the margin of error. (b), (c), and (d) are similar comparisons for the Aitken mode, accumulation mode and stratospheric coarse mode respectively (renaming from accumulation mode into the coarse mode does not exist in MAM4).

Figures 4(b), 4(c) and 4(d) respectively show the variations in stratospheric sulfate burdens of Aitken mode, accumulation mode and stratospheric coarse mode. The results used in these plots are three-day averages on every third day. In MAM4, most of the sulfate burden exists in the form of the accumulation mode, as renaming into the coarse mode is not available. Around November 15, 1991 (the time of peak stratospheric sulfate burden), Aitken mode

and accumulation mode contribute, respectively, 0.1% and 99.9% (0.3% and 99.7%) to total burden in MAM4SC (MAM4FC). For MAM5-PSA, the accumulation mode peaks briefly, but is soon almost entirely converted into the stratospheric coarse mode via renaming. Similar to the accumulation mode for MAM4, in both MAM5FC and MAM5SC the stratospheric coarse mode makes up more than 98% of the stratospheric sulfate burden on November 15, 1991, with about two-thirds of the remainder being in the accumulation mode and one-third in the Aitken mode.

It is worth noting that the peak values for the different aerosol modes do not occur concurrently. For the Aitken mode, all four experiments peak for the first time in late June and July (0.04 Tg S on June 30 in MAM4SC, 0.15 Tg S on July 30 in MAM4FC, 0.03 Tg S on June 30 in MAM5SC, and 0.1 Tg S on July 12 in MAM5FC). The results here agree with those in Fig. 2, where aerosol formation is faster in SC compared to FC, and MAM5FC is faster than MAM4FC due to replenishment of OH radicals. Several months after the Pinatubo eruption, there is again an increase in Aitken mode burden due to the eruption of Mount Hudson between August and October. The Mount Spurr and Lascar eruptions of 1992 and 1993 respectively are also visible here.

For the accumulation mode, the peak burden of 5.5 Tg S (4.8 Tg S) occurs on November 15 (November 30) in MAM4SC (MAM4FC). Much like for Aitken mode, the peak value for MAM4FC occurs later than MAM4SC as a result of the slower start in terms of sulfate formation. For MAM5-PSA, accumulation mode stratospheric sulfates are mostly transitory in nature, quickly renaming into the stratospheric coarse mode. The accumulation mode of MAM5SC and MAM5FC has small peak values of 0.4-0.8 Tg S during July 9-24. The stratospheric coarse mode burdens peak around November 15 for both MAM5-PSA experiments at around 5.5 Tg S.

Figure 5 shows the stratospheric burdens of sulfate for different modes and latitudinal regions of 30 °N-80 °N, 30 °S-30 °N, and 80 °S-30 °S. As ~~for~~ with Fig. 4, for all regions the vast majority of the stratospheric sulfate burden exists in the accumulation mode for MAM4 and in the stratospheric coarse mode for MAM5-PSA. It should be noted that the total stratospheric sulfate burden exhibits different changes with time for MAM5-PSA. Between 30 °S and 30 °N, the total stratospheric burden in all experiments declines the fastest compared to the other two regions due to both gravitational settling of sulfate and its poleward transport due to the Brewer-Dobson circulation. Between 30 °N-80 °N, the stratospheric sulfate burden peaks in February and March of 1992, as opposed to October 1991 in 30 °S-30 °N, due to the time required for aerosol transport northward via the Brewer-Dobson circulation. The stratospheric sulfate burden has a second peak in January 1993 at 30 °S-30 °N and 30 °S-80 °S corresponding to the Lascar eruption, though this does not counteract the overall decline over time. Between 30 °S-80 °S, the stratospheric sulfate burden peaks in November 1991 for both MAM5-PSA experiments, and afterwards remains relatively steady. For MAM5-PSA the stratospheric sulfate burden appears to oscillate annually in the southern hemisphere, with high values around October-November and low values around April of 1992 and 1993.

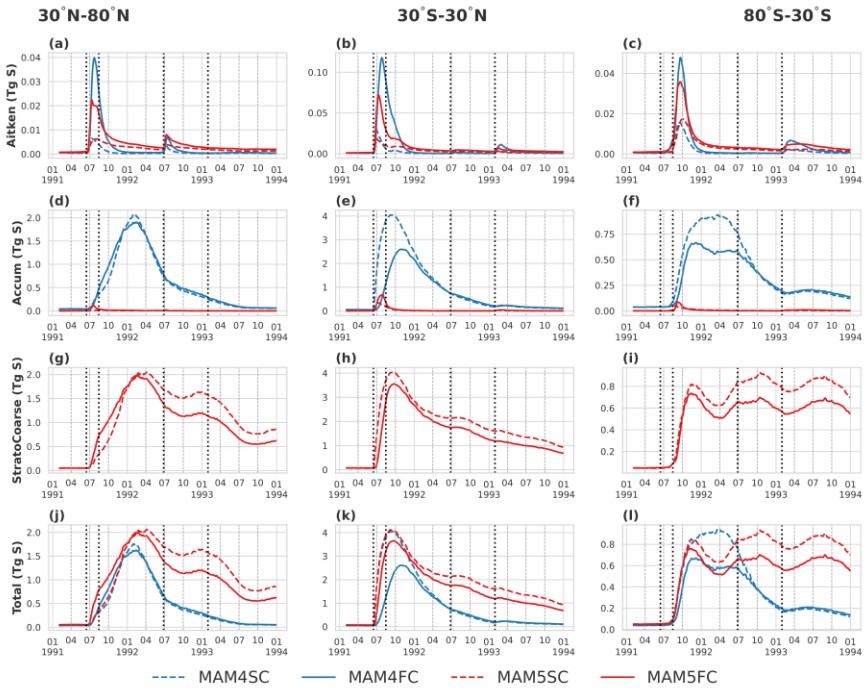

Figure 5: Simulated stratospheric sulfate burden (in Tg S) divided by mode and latitudinal region. The vertical lines represent the Pinatubo, Cerro Hudson, Spurr and Lascar eruptions respectively.

455 It can also be seen in Fig. 5 that the relative latitudinal contribution to the total stratospheric sulfate burden changes over time. The burden between 30 °S and 30 °N constitutes about two-thirds or more of the stratospheric sulfate burden in the months after the Pinatubo eruption. Starting from April of 1992, the stratospheric burden of 1.7-2.1 Tg S between 30 °N-80 °N is similar in magnitude to the stratospheric burden between 30 °S and 30 °N in all four experiments. Starting from 1993, the stratospheric burden south of 30 °S in MAM5-PSA begins to make up a much larger portion 460 of the total between 80 °S and 80 °N (about 0.8 Tg S out of the total of about 4.1 Tg S), due to the stratospheric coarse mode burdens not decreasing. This accounts for the slower decline of the total stratospheric burden in MAM5-PSA as seen in Fig. 4(a).

Since the independent stratospheric coarse mode is newly added in this study, Figure 6 depicts the distribution of 465 MAM5-PSA aerosol volume particle size distribution, as compared with WOPC observations (Deshler et al., 1993; Deshler et al., 2003). MAM4 has been omitted as it does not include coarse mode sulfate. It can be seen that with the exception of December 30, 1991, MAM5FC generally better matches WOPC observations in terms of coarse mode mass than MAM5SC. However, MAM5FC coarse mode size is biased towards being smaller than the observations.

The relatively smaller coarse mode aerosols may also help to explain the excessively long lifespan later seen past 1992 in Figs. 4 and 5.

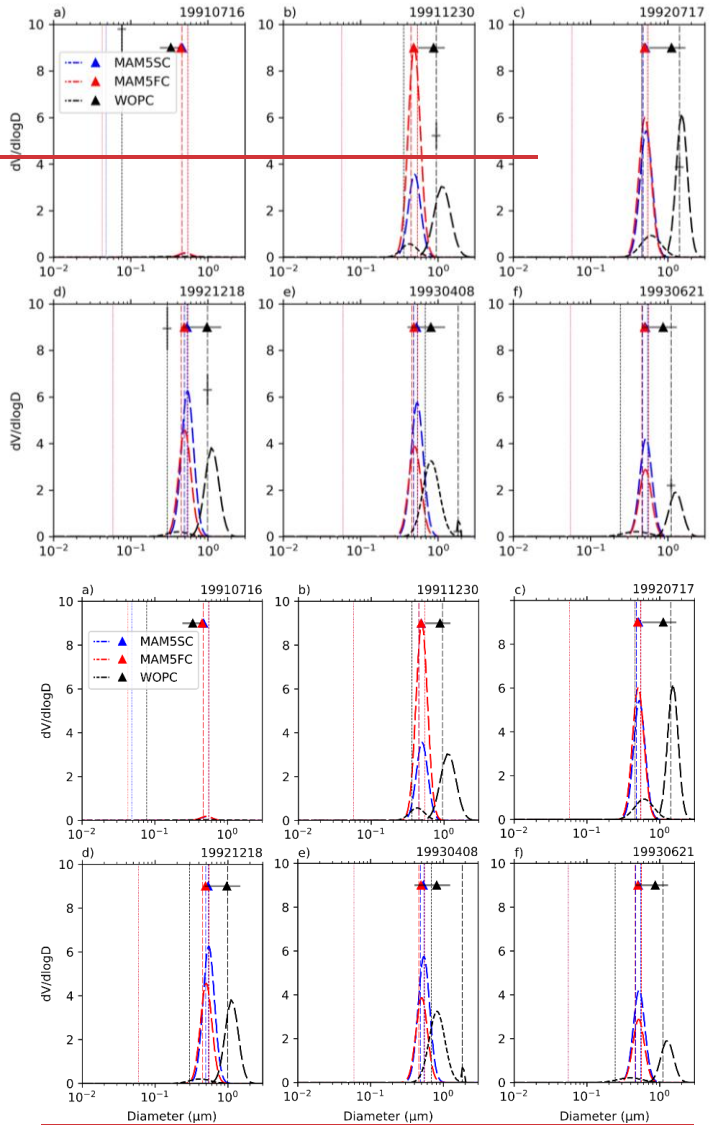

Figure 6: Comparisons of stratospheric aerosol size distributions from MAM5SC and MAM5FC with observations from WOPC for 1991–1993. WOPC launches are samples taken from the 18 km measurements and matched to the nearest model height and grid cell over Laramie, Wyoming (41.3° N, 105° W). The vertical dotted, dashed and long dashed lines ~~with longer dashes~~ represent the ~~accumulation mode's~~ geometric mean ~~diameter, while~~diameters of the ~~vertical lines with~~

~~shorter dashes represent the~~Aitken, accumulation and stratospheric coarse ~~mode's geometric mean diameter~~modes respectively**. The triangles represent the effective diameters calculated from the size distribution.**

3.3 Process analyses

In order to better understand the differences between the experiments and how the aerosols transition between the different modes, the tendencies (i.e., the rate of mass change into or out of a certain mode) between 80 °S and 80 °N are plotted in Fig. 7. The left column represents the tendencies over time, while the right column represents the cumulative tendency, integrated over time. The tendencies are integrated over the three dimensions of: all longitudes, the above-mentioned latitude range, and vertically above the tropopause. Here it is assumed that these rates apply only to sulfate and other aerosol contributions are negligible within the stratosphere. As described in the methodology section 2.1, nucleation, coagulation and renaming represent mass exchange between the different aerosol modes. Condensation represents the mass growth within the same aerosol mode.~~The tendencies are integrated over the three dimensions of: all longitudes, the above-mentioned latitude range, and vertically above the tropopause.~~

~~The magnitude of the tendency for the formation of Aitken mode aerosols through the nucleation of gaseous H_2SO_4 (NUCL) is generally higher in the FC experiments compared to the SC experiments, which explains the higher Aitken mode sulfate concentrations in FC than in SC as shown in Fig. 3. For MAM4FC, the peak value occurred on July 24 and it does not return to background levels until early December 1991. MAM5FC peaks on July 3 and returns to background levels after the middle of August 1991. In both MAM4SC and MAM5SC, the rate peaks on June 24 and returns to background levels by the start of August 1991. Due to the higher OH concentrations in the SC experiments, the nucleation process begins and ends earlier in the SC experiments compared to FC. Considering the cumulative mass changes depicted in Fig. 7(b), the curves for the SC experiments flatten out earlier than those for FC (i.e., the microphysical process in SC is mostly concluded). For MAM4SC (MAM5SC) the curve flattens out by July 15, 1991 (July 6, 1991), with later, less significant processes contributing to a 39.4% (63.8%) increase by the end of 1993. For MAM4FC (MAM5FC) the curve flattens out by October 19, 1991 (September 16, 1991), with approximately a 9.3% (10.8%) increase by the end of 1993. Note that there was some interference from the Mount Hudson eruption in August 1991, as well as Spurr and Lascar. The total magnitude of the nucleation process is also different between the experiments, with MAM4SC, MAM4FC, MAM5SC and MAM5FC reaching roughly 0.3, 1.3, 0.1 and 0.6 Tg respectively by the end of 1993.~~

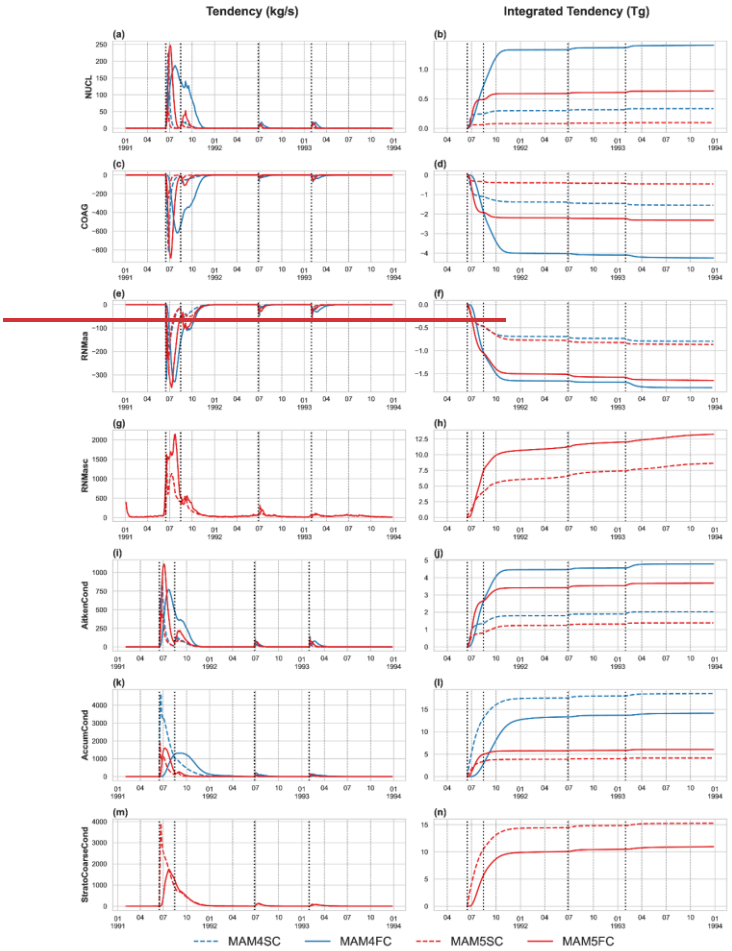

~~Figure 7: The relevant tendencies for each mode in each experiment in the stratosphere between 80°S and 80°N. See Figure 1(a) for description of processes. Positive values represent gained mass from the associated microphysical process from the perspective of the aerosol mode in question. NUCL represents the aerosol mass gain for Aitken mode due to nucleation (i.e., aerosol formation), COAG represents Aitken mode mass loss due to coagulation into the accumulation mode, RNMaa represents Aitken mode mass loss due to renaming into the accumulation mode, RNMasc represents the gain in mass for stratospheric coarse mode in MAM5 PSA due to renaming from the accumulation mode. The left column plots represent the tendency values over time, while the right column represents the cumulative mass change due to the associated microphysical process (i.e. tendency integrated over time). The bottom three rows represent the condensation tendencies for each mode, with the positive value representing mass transition from gaseous phase to the aerosol. The vertical lines represent the Pinatubo, Cerro Hudson, Spurr and Lascar eruptions respectively.~~

Figs. 7(c)(d) show the aerosol mass loss rates (negative values) of the Aitken mode due to coagulation into the accumulation mode (COAG). Generally, the peak values occur some time (0 to 9 days) after that of the nucleation process, as coagulation becomes stronger when Aitken mode aerosol concentrations are high and accumulation mode aerosols become available. This happens sooner for the SC experiments than FC (June 27 for MAM4SC vs. August 2 for MAM4FC, June 24 for MAM5SC vs. July 6 for MAM5FC). For the integrated values (Fig. 7(d)), much like in the nucleation process, MAM4 has stronger coagulation than MAM5-PSA, and FC has stronger coagulation than SC. The curves also flatten slightly later than for the nucleation process, about 0 to 9 days after the corresponding curve for nucleation as described above. The total magnitude from largest to smallest is still MAM4FC, MAM5FC, MAM4SC and MAM5SC, at 4 Tg, 2.2 Tg, 1.2 Tg and 0.4 Tg, respectively.

Figs. 7(e)(f) show the aerosol mass loss rate of the Aitken mode due to renaming into the accumulation mode (RNMaa). This occurs concurrently with the coagulation process, though the peak occurs slightly earlier as it only requires the presence of Aitken mode aerosols and not accumulation mode aerosols. MAM4SC, MAM4FC, MAM5SC, and MAM5FC peak on June 18, July 21, June 27, and July 12, respectively. Of particular note is that the response to the Cerro Hudson eruption appears to be much stronger here than in the other processes, and that the difference between MAM4 and MAM5-PSA is small for both FC and SC.

Figs. 7(g)(h) represent the aerosol mass gain rate of the stratospheric coarse mode due to renaming from the accumulation mode (RNMasc). This step occurred after most of the above processes had passed their peaks and accumulation mode aerosols had grown considerably in size. MAM5SC peaked on July 9 while MAM5FC peaked on July 24. Unlike the other processes, in both MAM5SC and MAM5FC the curve in Fig. 7(h) does not flatten, and the renaming process does not completely conclude at the end of January 1993 (explained above in Fig. 5 discussion).

Figs. 7(i)-(n) represent the condensation processes for each of the three modes. In general, this accounts for the changes in mass within each mode, though the mass of each mode is still not strictly conserved due to exchanges between the troposphere and stratosphere. It can be seen that FC has stronger condensation tendencies than SC in the Aitken mode due to the larger amount of Aitken mode aerosols seen in Figure 5. Accumulation mode tendencies are stronger for MAM4 than MAM5-PSA likewise due to very small accumulation mode concentrations in MAM5-PSA. MAM5SC has a much stronger condensation tendency than MAM5FC for the stratospheric coarse mode, which appears to counterbalance the differences in RNMasc, ultimately leading to relatively close stratospheric coarse mode burdens between the two experiments. Similarly, MAM4SC has stronger condensation tendency for the accumulation mode than MAM4FC throughout the span of the experiment. This suggests that in SC, H_2SO_4 within the stratosphere tends to directly contribute to accumulation/stratospheric coarse mode mass through condensation, whereas in FC the H_2SO_4 contributes a larger portion to stratospheric burden through nucleation and condensation onto the Aitken mode, which eventually grow to accumulation/coarse mode through renaming and coagulation (though the majority of condensation still occurs in the final accumulation/stratospheric coarse mode).

~~Overall, these processes are delayed in FC compared to SC, though the delay is smaller in MAM5FC compared to MAM5SC due to OH replenishment. The full chemistry experiments also have stronger nucleation, coagulation and renaming processes with larger changes in aerosol mass due to these processes compared to the corresponding simple chemistry experiments. In conjunction with the stratospheric burden plotted in Fig. 4, this suggests that removal processes are also stronger in the full chemistry experiments. MAM4 also generally has stronger nucleation leading to higher Aitken mode concentrations, and therefore also has stronger coagulation processes than MAM5-PSA.~~

With respect to nucleation, Figure 7(a) shows the magnitude of the tendency for the formation of Aitken mode aerosols through the nucleation of gaseous H_2SO_4 (NUCL) is generally higher in the FC experiments compared to the SC experiments, which leads to the higher Aitken mode sulfate concentrations in FC than in SC as shown in Fig. 4(b). Although one would expect SC to have faster nucleation without the bottleneck of OH concentrations, new particle formation by nucleation competes against aerosol growth by condensation. Condensation is stronger in the SC experiments than FC for the first five months after the eruption, predominantly in the accumulation mode condensation for MAM4 (Figs. 8 (c)(d)) and in the stratospheric coarse mode for MAM5-PSA (Figs. 8 (e)(f)). This leads to competition with the nucleation process, so FC has stronger nucleation than SC. Due to the higher OH concentrations in the SC experiments, the nucleation process begins and ends earlier in the SC experiments compared to FC. Considering the cumulative mass changes depicted in Fig. 7(b), the curves for the SC experiments flatten out (i.e., the microphysical process in SC is mostly concluded) earlier than those for FC.

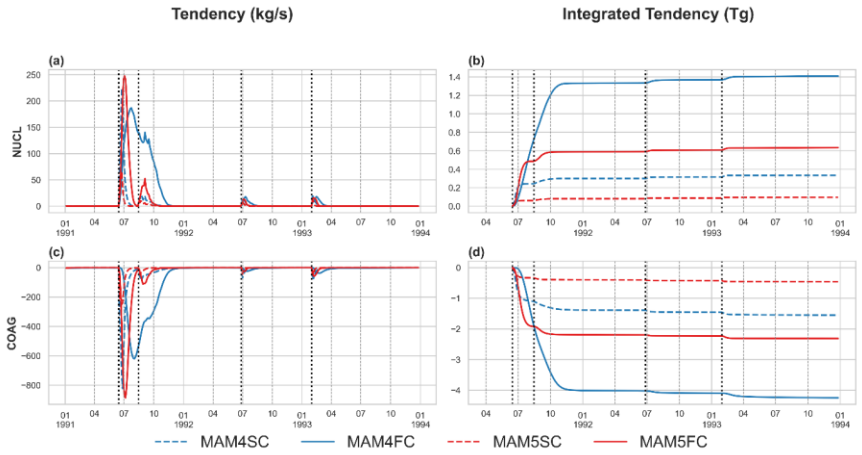

Figure 7: A series of figures for the relevant tendencies for each mode in each experiment in the stratosphere between 80°S and 80°N., in terms of aerosol mass. See Figure 1(a) for description of processes. Positive values represent gained mass from the associated microphysical process from the perspective of the aerosol mode in question. NUCL represents the aerosol mass gain for Aitken mode due to nucleation (i.e., aerosol formation), COAG represents Aitken mode mass loss due to coagulation into the accumulation mode. The left column plots represent the tendency values over time, while the right column represents the cumulative mass change due to the associated microphysical process (i.e. tendency integrated over time). The vertical lines represent the Pinatubo, Cerro Hudson, Spurr and Lascar eruptions respectively.

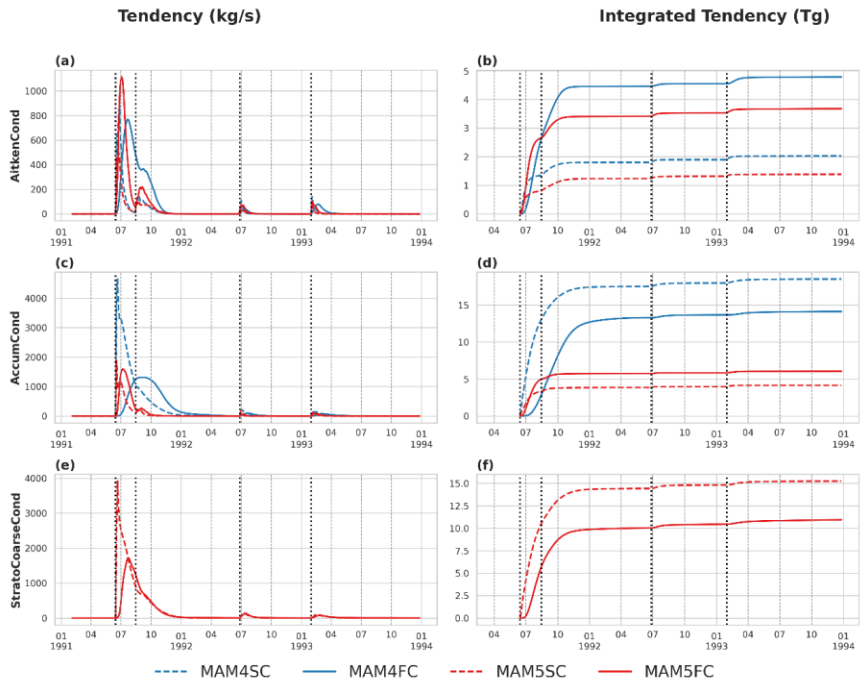

Figure 8: Tendency plots for condensation in the different aerosol modes, similar to those for nucleation and coagulation in Fig. 7. Positive values represent mass transition from the gaseous phase to the aerosol.

With respect to coagulation, Figs. 7(c)(d) show the aerosol mass loss rates (negative values) of the Aitken mode due to coagulation into the accumulation mode (COAG). The magnitude of the coagulation generally follows that of the nucleation process, as the strength of the coagulation process is proportional to Aitken mode aerosol number and mass.

With respect to the condensation processes, Figs. 8(a)-(f) show the condensation processes for each of the three modes. Fig. S6 in the supplementary shows the sum of condensation processes across the three modes for reference. Across the first five months after the eruption, for Aitken mode condensation, FC has stronger condensation tendencies than SC corresponding to the larger burden of Aitken mode aerosols seen in Figure 4(b). For the accumulation mode, condensation is stronger for MAM4 than MAM5-PSA likewise corresponding to the very small accumulation mode burden in MAM5-PSA (Fig. 4(c)). For the stratospheric coarse mode, MAM5SC has a much stronger condensation tendency than MAM5FC corresponding to the former having a higher stratospheric coarse mode burden (Fig. 4(d)). It should be noted that MAM4SC similarly has stronger condensation tendency for the accumulation mode than MAM4FC, as the sulfate does not grow beyond the accumulation mode. After five months, condensation concludes in all of the experiments except for MAM4FC, due to delays from its OH bottleneck.

Figs. 9(a)(b) show the aerosol mass loss rate of the Aitken mode due to renaming into the accumulation mode (RNMaa). Similar to coagulation above, the strength of RNMaa is also dependent on the preceding processes of nucleation and condensation, which provide the large Aitken mode particles necessary for renaming. Since nucleation and Aitken mode condensation is stronger in FC than the SC experiments, this is also true for RNMaa.

Figs. 9(c)(d) represent the aerosol mass gain rate of the stratospheric coarse mode due to renaming from the accumulation mode (RNMasc). Similar to RNMaa, the relative strength is determined by the prior steps, here being RNMaa, COAG and AccumCond, leading to MAM5FC being stronger than MAM5SC.

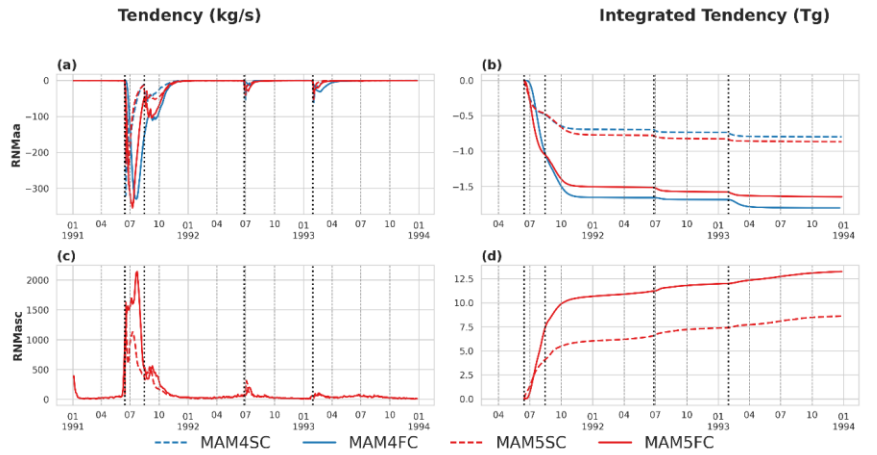

Figure 9: Tendency plots for renaming, i.e. the transition of mass between aerosol modes due to the aerosol population reaching a prerequisite size, as described in Figure 1(a). RNMaa represents the mass transition from the Aitken mode to the accumulation mode (renaming is only possible in this direction, and cannot occur in the reverse), and the negative value represents the mass loss of the Aitken mode. RNMasc represents the mass transition from the accumulation mode to the stratospheric coarse mode (also only possible in this direction), and the positive value represents the mass gain of the stratospheric coarse mode.

Overall, SC has stronger condensation processes (sum for all modes) and weaker nucleation (i.e. initial formation of Aitken mode sulfates) relative to FC over the first five months, again showing the competition between condensation and nucleation for H_2SO_4. Because coagulation and renaming are dependent on nucleation and condensation, FC is stronger than SC for coagulation and renaming. With respect to the differences in processes between MAM4 and MAM5-PSA, MAM4 has stronger nucleation, coagulation and renaming processes due to weaker competition from condensation.

Formatted: Centered

We have also examined the microphysical processes divided by latitudinal regions (Supplementary Figs. ~~5~~ 7 and ~~6~~8). The same patterns as above apply between 30 °S and 30 °N. Above 30 °N and below 30 °S the same signal from the Pinatubo is still present, though slightly delayed due to the time that it took for the aerosol to transport poleward. Signals from other eruptions (Spurr and Lascar) are also present. The main difference is in RNMasc. Above 30 °N and below 30 °S, renaming into the stratospheric coarse mode for MAM5-PSA continues long after the Pinatubo eruption, contributing to the long lifespan of stratospheric sulfate in MAM5-PSA as depicted in Figures 4 and 5. This did not occur between 30 °N and 30 °S, where the stratospheric burden also declines more rapidly as seen in Fig. 5. It is also worth noting that the same pattern does not exist for the other tendencies, and only RNMasc continues to a significant degree past 1992. The condensation tendencies are also not evenly divided across different latitudinal regions, with 30 °S-80 °S and 30 °N-80 °N having stronger condensation tendencies for MAM4FC in the Aitken and accumulation modes, and for MAM5FC in the Aitken and stratospheric coarse modes. Notable increases in condensation can be seen during the Spurr and Lascar eruptions, though it may also be due to Aitken mode aerosols from the original Pinatubo eruption being transported away from the equator and continuing their growth elsewhere.

3.4 Simulated AOD and net solar flux

Figure 10~~8~~ depicts the anomaly of simulated AOD from the four experiments and AVHRR observations from 1991-1993, ~~normalized~~relative to the corresponding data from 1989 (i.e., the monthly averages during 1991-1993 subtracted by the corresponding monthly average in 1989 for the same pixel), and masked according to the observed area by AVHRR. The AVHRR AOD anomaly had a maximum value in the range of 0.4-0.45 between 10 °N and 10 °S starting from July 1991, corresponding to the Pinatubo eruption. The four simulations do not have as high of an AOD anomaly for the Pinatubo eruption, with an anomaly of 0.25-0.3 for MAM4SC, 0.15-0.2 for MAM4FC, and 0.35-0.4 for both MAM5SC and MAM5FC experiments. In this respect, MAM5-PSA better captures the AOD anomaly due to the Pinatubo eruption. The simulated AOD maximums occurs slightly north of the equator, to the north of the AOD maximum in the AVHRR observation.

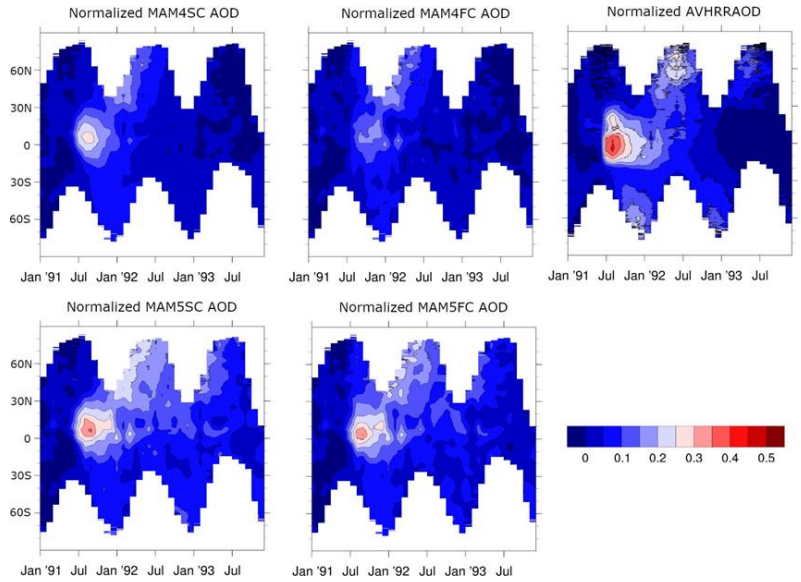

Figure ~~8~~10: Latitude vs. time plots of model simulated AOD and AVHRR observed AOD~~. Both were normalized~~ anomaly values relative to 1989 AOD output or observations respectively, to eliminate contributions from the troposphere and background stratospheric AOD. Model output was masked to correspond to areas that AVHRR had observation data for. Results were averaged across longitude.

The four experiments capture well the northward transport of the AOD anomaly in the latter half of 1991 and the first half of 1992, also matching the generally higher stratospheric sulfate burden above 30 °N compared to below 30 °S (Fig. 5). In all four experiments and the AVHRR observations, the AOD anomaly diminished over time following the Pinatubo eruption, returning towards 0 starting from 1993. This decay is weaker in the MAM5-PSA experiments compared to MAM4 and the AVHRR results, with lingering positive AOD anomalies of 0.05-0.1 throughout 1993, matching the longer lifespan of the stratospheric sulfate in MAM5-PSA as seen in Fig. 4.

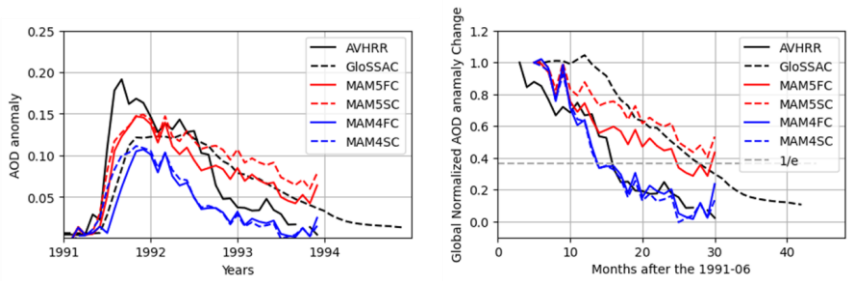

Figure ~~9~~11: Comparison of AOD anomaly between simulations and observations. The left panel shows the time evolution of monthly AOD anomaly values from simulations and AVHRR and GloSSAC observations, while the right panel shows the time evolution of normalized AOD anomaly.

We have evaluated the characteristics of the time evolution of simulated global AOD anomaly and its e-folding time against observational data. The time evolution of global monthly AOD anomaly, averaged between 60°S–60°N, is depicted in the left panel of Fig. 11~~9~~. The AVHRR and the Global Space-based Stratospheric Aerosol Climatology (GloSSAC) were two satellite-based AOD observations that provided global coverage during the Mt. Pinatubo eruption. GloSSAC offered zonal values with a latitudinal resolution of 5° and uniform spatio-temporal coverage up to the year 1994. However, due to instrument saturation for optical depths around 0.15, GloSSAC was less accurate in the center of tropical clouds during the first months after the Mt. Pinatubo eruption. Conversely, AVHRR could only measure stratospheric AOD values larger than 0.01, making it less reliable when AOD values were low (Russell et al., 1996; Quaglia et al., 2023). To calculate AOD anomaly values, background levels (from June 1989 to May 1991) were removed from both observations and simulations. The MAM5FC and MAM5SC simulations produced a reasonable global mean AOD anomaly peak of around 0.15 in November 1991, when the simulated sulfate aerosol burden peaked (Fig. 4). These peaks were higher than the GloSSAC peak (0.12) but lower than the AVHRR peak (0.19). The MAM4FC and MAM4SC simulations produced AOD anomaly peaks (0.11) that were smaller than GloSSAC, indicating an apparent underestimation of AOD anomaly strength. The MAMFC simulation showed a faster AOD anomaly decay than MAM5SC, with values aligning closely with GloSSAC in 1993. In contrast, the MAM4FC and MAM4SC simulations consistently underestimated AOD anomaly compared to GloSSAC from October 1991 to December 1993.

The e-folding time, calculated as the time between the maximum and the 1/e value, was 13 months in AVHRR and ~~23~~16 months in GloSSAC. The difference between the two measurements is due to the nature of these instruments. The simulated e-folding time in MAM4FC and MAM4SC was 10 months, while MAM5FC and MAM5SC had e-folding times of 19 months and 25 months, respectively. Compared to a previous study (11 to 15 months, Quaglia et al. (2023)), the MAM5FC e-folding time is larger but remains within a reasonable range.

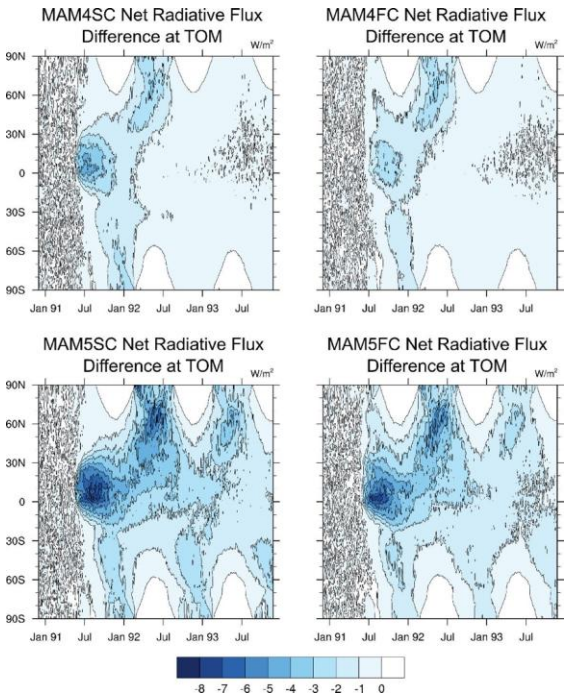

Figure ~~10~~12: Latitude vs. time plots of the top-of-model net radiative flux difference between the four experiments and corresponding model simulations with emissions from volcanic eruptions shut off. Units in W/m^2.

Figure 1~~2~~0 depicts the differences in the top-of-model net solar flux in the four experiments with and without the emissions from volcanic eruptions (negative values representing cooling from the volcanic aerosol). The location of the maximum of the net solar flux difference agrees well with the location of the AOD anomalies in Fig. 1~~0~~8. The maximum of the net solar flux is simulated to be about -6 W/m^2 for MAM4SC, -4 W/m^2 for MAM4FC, and -10 W/m^2 for both MAM5-PSA experiments. Considering the more accurate AOD simulation in MAM5-PSA, it is expected that MAM5-PSA also better captures climate effects from the Pinatubo eruption. The time variations of the global mean top-of-model net radiative flux shows that, during October-November of 1991, MAM4 experiments produce weaker peak values of around -1.5 W/m^2 while MAM5-PSA produces peak values of roughly -3.0 W/m^2 (Fig. 1~~3~~1). The latter results agree closely with the those simulated by CESM experiments in Mills et al. (2017) as well as the E3SMv2-SPA ~~modified MAM4~~ results from Brown et al. (2024), where the peak values are also roughly -3.0 W/m^2. It also agrees well with the simulation results from Hansen et al. (2005) up to early 1992, which also reports a peak value of about -3.0 W/m^2 across their five runs, though the net radiative flux signal is slower to diminish around July 1992, concurring with the stratospheric sulfate burden depleting too slowly in MAM5FC. In general, the net radiative flux differences closely follow the same patterns as the stratospheric sulfate burden depicted in Fig. 4, suggesting that

differences in chemistry between SC and FC, and the additional stratospheric coarse mode in MAM5-PSA, first influence stratospheric sulfate burdens, which in turn affect the net radiative flux.

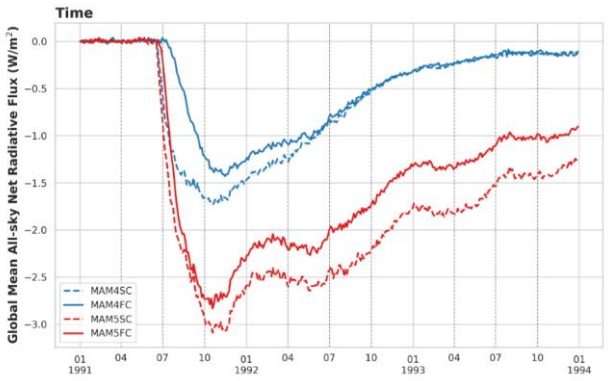

Figure ~~11~~13: Global mean net radiative flux anomaly in the four experiments, where negative values represent a net upward flux. The anomaly is the difference with the corresponding model experiment with the volcanic emissions shut off.

4 Conclusions and discussions

~~In this work, we have described an implementation of a 5-mode version of the Modal Aerosol Module (MAM5-PSA) used in E3SMv2 as well as a more complex "full chemistry" set-up, resolving issues in simulating the coarse mode for stratospheric sulfate seen in previous studies. The intention is to provide more accurate simulations of the chemical and microphysical processes within the stratosphere following the Pinatubo eruption, and to compare it against a simulation using simplified chemistry and the default MAM4 aerosol module. Full chemistry in MAM5-PSA includes the addition of a series of chemical reactions which allow the simulation of OH radical replenishment compared to that in MAM4. MAM5-PSA adds a stratospheric coarse mode that specifically represents the microphysical properties of stratospheric sulfate. In particular, the geometric standard deviation is smaller, contributing to a longer lifespan for stratospheric sulfate aerosol. Corresponding to these changes, we carried out four experiments: MAM4SC, MAM4FC, MAM5SC and MAM5FC to simulate the burdens, AOD, and radiative effect of volcanic aerosols following the Pinatubo eruption.~~

~~These changes led to large differences in both the temporal variations and the spatial distributions of sulfate concentrations. Directly after the eruption, the SC experiments had the fastest rise in sulfate concentrations, as FC was limited by OH required to oxidize SO_2. MAM5FC was significantly faster than MAM4FC however due to the OH radical replenishment. Vertically, sulfate distributions were generally at lower altitudes in FC compared to SC, caused by the differences in SO_2, OH, and specific humidity within the stratosphere. With respect to the stratospheric sulfate burden, MAM5FC agreed best with the HIRS observations from the eruption of the volcano to the end of 1992.~~

~~Starting in 1993, stratospheric sulfate burdens in all four of the experiments began to diminish, but the process was slower in MAM5-PSA because of the stronger deposition in MAM4 relative to MAM5-PSA. The slow removal of stratospheric sulfate burden in MAM5-PSA occurs mostly in the high latitudes but is faster near the equator. With respect to the stratospheric sulfate burden, MAM5FC agreed best with the HIRS observations from the eruption of the volcano to the end of 1992. Compared to WOPC observations, MAM5-PSA has comparable mass in the coarse mode, but coarse mode particles are smaller, which may be responsible for the longer lifespan of stratospheric sulfate after the start of 1993. We assessed the time evolution and e-folding time of simulated global AOD anomaly against satellite observations (AVHRR and GloSSAC). The MAM5FC and MAM5SC simulations generally produced reasonable AOD peaks and decay patterns, while MAM4FC and MAM4SC tended to underestimate AOD strength and overestimate the decay rate.~~

~~We further analyzed the tendencies associated with the microphysical processes related to the growth of stratospheric sulfate: nucleation (NUCL), coagulation (COAG), condensation (AitkenCond, AccumCond, StratoCoarseCond), and renaming (RNMaa and RNMasc). In general, all of these processes are stronger in FC than in SC. For condensation, FC is stronger than SC in the Aitken mode due to the higher concentrations of Aitken mode sulfate, and MAM4 is stronger than MAM5-PSA in the accumulation mode again due to higher concentrations. It should be noted that the differences in integrated tendencies between the experiments were often much larger than the differences in stratospheric sulfate burdens between the experiments, which suggested that sedimentation was faster in FC than in SC to counterbalance the stronger aerosol production suggested by the stronger tendencies. In terms of timing, the tendencies generally initiate and conclude faster in SC compared to FC due to not having limitations for OH radicals, which correspond well with the occurrence of peaks of sulfate burden. Overall, in terms of accurately portraying the retention of sulfate aerosols in the stratosphere, MAM5-PSA provides a substantial improvement over MAM4 during 1992.~~

~~We compared the model output AOD against AVHRR observations to assess overall performance. Immediately after the eruption, MAM5-PSA performs better than MAM4 by producing AOD anomalies closer to AVHRR. In all four experiments, the northward transport of aerosols due to the Brewer-Dobson circulation was accurately captured, but the AOD related to the Cerro Hudson and Spurr eruptions was not distinct compared to AVHRR. These eruptions have a much lower injection height than Pinatubo (11-16 km and 9-14.5 km altitude respectively) and a much smaller emission of SO_2 which may explain the lack of a signal. In terms of the changes in global mean net radiative flux, the simulated largest global mean values following the eruption were roughly -1.5 W/m^2 during October-November of 1991 in MAM4 experiments and about -3 W/m^2 in MAM5-PSA experiments. MAM5-PSA results were much closer to the number seen in Mills et al. (2017) and Brown et al. (2024), also roughly -3 W/m^2.~~

In this work, we have implemented a fifth stratospheric coarse mode (MAM5-PSA) on top of the original four-mode version Modal Aerosol Module (MAM4) used in E3SMv2. We also consider a more complex "full chemistry (FC)" set-up, which includes the addition of a series of chemical reactions which allow the simulation of OH radical replenishment compared to "simple chemistry (SC)" with prescribed OH concentrations. We have carried out a series

of simulations of the Pinatubo eruption for the time period of 1991-1993 to better understand the aerosol microphysical processes including nucleation, coagulation and condensation. We have also compared model simulation results with measurements of stratospheric sulfate burden, aerosol size, AOD and net radiative flux.

Compared to SC, FC leads to large differences in both the temporal variations and the vertical distributions of sulfate concentrations. Directly after the eruption, the SC experiments had the fastest increase in sulfate concentrations, as FC was limited by OH required to oxidize SO_2. The increase in MAM5FC was significantly faster than MAM4FC however due to the OH radical replenishment. Vertically, sulfate distributions were generally at lower altitudes in FC compared to SC, caused by the differences in SO_2, OH, and specific humidity within the stratosphere. Starting in 1993, stratospheric sulfate burdens in all four of the experiments began to diminish, but the process was slower in MAM5-PSA because of the stronger sedimentation in MAM4 relative to MAM5-PSA. The slow removal of stratospheric sulfate burden in MAM5-PSA occurs mostly in the high latitudes but is faster near the equator.

Model evaluations indicate that the simulation with both MAM5-PSA and full chemistry (i.e. MAM5FC) can better capture observations such as sulfate burden, aerosol size, AOD and net radiative flux. With respect to the stratospheric sulfate burden, MAM5FC (compared to MAM4SC, MAM4FC and MAM5SC) agreed best with the HIRS observations from the eruption of the volcano to the end of 1992. Compared to WOPC observations of aerosol size, MAM5FC better captures observations and has comparable mass in the coarse mode. We also assessed the time evolution and e-folding time of simulated global AOD anomaly against satellite observations (AVHRR and GloSSAC). The MAM5FC and MAM5SC simulations generally produced reasonable AOD peaks and decay patterns, while MAM4FC and MAM4SC tended to underestimate AOD strength and overestimate the decay rate. From July 1991 to the end of 1992, simulated net radiative flux anomalies are in the range of -2.8 to -1.3 W/m^2, agreeing well with observed net radiative flux anomalies within the range of -3.8 to -1 W/m^2 (Brown et al., 2024).

We further analyzed the tendencies associated with the microphysical processes related to the growth of stratospheric sulfate: nucleation (NUCL), coagulation (COAG), condensation (AitkenCond, AccumCond, StratoCoarseCond), and renaming (RNMaa and RNMasc). Due to the limited amount of H_2SO_4 in the stratosphere, the nucleation and condensation processes compete over H_2SO_4 until condensation ceases about five months after the eruption. Overall, over these five months, FC has weaker condensation processes (sum for all modes) and consequently stronger nucleation, coagulation and renaming relative to SC, since coagulation and renaming are dependent on nucleation and condensation.

The usage of the Modal Aerosol Module in this study allows us to more accurately reflect the aerosol growth process over time. For the purpose of simulating volcanic eruptions, this is an improvement over bulk schemes which cannot represent aerosol size (Gao et al., 2023) and allows for more accurate simulation of aerosol lifespan. Similar to (Brown et al., 2024) and (Mills et al., 2016), issues with the excessively short lifespan of stratospheric sulfates in default MAM (i.e. MAM4 in this study) are addressed with modifications of aerosol size parameters to better reflect coarse mode

stratospheric sulfates. However, instead of overwriting the original coarse mode properties and interfering with the simulation of other coarse mode aerosols like sea salt and dust, we separate stratospheric sulfate into its own mode. This not only prevents interference with the other coarse mode aerosols, but also allows us to investigate the aerosol microphysical processes of sulfates in particular.

A number of factors contribute to the uncertainty of our results. One important factor is the known dry bias in E3SM's stratosphere (Christiane Jablonowski, personal communication, 2024), since water vapor plays an important role in the HO_x cycle relevant to the initial sulfate formation, as well as later sulfate growth and sedimentation. Another issue is the presence of minor volcanic eruptions such as Cerro Hudson, Spurr and Lascar, which produced much less SO_2 than Pinatubo, but still significant enough to leave a distinguishable signal following Pinatubo's eruption. A third factor is the interaction between the Pinatubo eruption and stratospheric ozone. Volcanic eruptions are known to affect stratospheric ozone concentrations (Peng et al., 2023) directly and indirectly through factors such as the decreases in tropospheric temperatures, modified circulation and the changes in the stratospheric chemical composition (Dhomse et al., 2015). The capabilities of E3SM in simulating stratospheric ozone in the unique circumstances of a volcanic eruption are not well studied. Further understanding of these factors would greatly aid in the accurate simulation of Pinatubo and other volcanic eruptions.

In summary, our study shows that a physical representation of aerosol size distribution while also considering the impact of interactive OH concentrations can better capture observations of stratospheric sulfate burden, aerosol size, AOD and net radiative flux, which have important implications for future studies of stratospheric aerosols.

Formatted: Font color: Auto

Code and data availability.

AVHRR observational data was downloaded from https://www.ncei.noaa.gov/data/avhrr-aerosol-optical-thickness/access. The VolcanEESM emissions files used in this study can be found at https://svn-ccsm-inputdata.cgd.ucar.edu/trunk/inputdata/atm/cam/chem/stratvolc/. The source code and run scripts used in this study can be found at https://zenodo.org/doi/10.5281/zenodo.12734295.

Author contributions.

Conceptualization: AH, XL and ZK. Data curation: AH, ZK and BW. Formal analysis: AH. Funding acquisition: XL, DB and KP. Investigation: AH. Methodology: AH, XL and ZK. Project administration: XL, HW, SX, DB and KP. Resources: XL, DB and KP. Software: AH implemented MAM5-PSA into E3SMv2 with assistance from ZK, MW, BW and ZL. Original MAM5-PSA implementation in E3SMv1 by ZK. ZK, MW, HW and QT enabled and improved the chemistry scheme that "full chemistry" is based on. Supervision: XL, DB and KP. Validation: AH. Visualization: AH. Writing – original draft preparation: AH. Writing – review and editing: all authors.

Competing interests.

Some authors are members of the editorial board of Atmospheric Chemistry and Physics.

Disclaimer.

Acknowledgements.

XL, AH, BW, HB, DB, and KP acknowledge the support of this work by the Laboratory Directed Research and Development program at Sandia National Laboratories, a multimission laboratory managed and operated by National Technology and Engineering Solutions of Sandia, LLC., a wholly owned subsidiary of Honeywell International, Inc., for the U.S. Department of Energy's National Nuclear Security Administration under contract DE-NA-0003525. XL, ZK, ZL, MW, HW, QT, and SX acknowledge the support by the U.S. Department of Energy (DOE), Office of Science, Office of Biological and Environmental Research, Earth and Environmental System Modeling program as part of the Energy Exascale Earth System Model (E3SM) project. The work at the Lawrence Livermore National Laboratory (LLNL) was performed under the auspices of the U.S. DOE by LLNL under Contract DE-AC52-07NA27344. The Pacific Northwest National Laboratory (PNNL) is operated for DOE by Battelle Memorial Institute under contract DE-AC05-76RLO1830.

References

Aubry, T. J., Engwell, S., Bonadonna, C., Carazzo, G., Scollo, S., Van Eaton, A. R., Taylor, I. A., Jessop, D., Eychenne, J., Gouhier, M., Mastin, L. G., Wallace, K. L., Biass, S., Bursik, M., Grainger, R. G., Jellinek, A. M., and Schmidt, A.: The Independent Volcanic Eruption Source Parameter Archive (IVESPA, version 1.0): A new observational database to support explosive eruptive column model validation and development, Journal of Volcanology and Geothermal Research, 417, 107295, https://doi.org/10.1016/j.jvolgeores.2021.107295, 2021.

Baran, A. and Foot, J.: New application of the operational sounder HIRS in determining a climatology of sulphuric acid aerosol from the Pinatubo eruption, Journal of Geophysical Research: Atmospheres, 99, 25673-25679, 1994.

Bergman, T., Kerminen, V. M., Korhonen, H., Lehtinen, K. J., Makkonen, R., Arola, A., Mielonen, T., Romakkaniemi, S., Kulmala, M., and Kokkola, H.: Evaluation of the sectional aerosol microphysics module SALSA implementation in ECHAM5-HAM aerosol-climate model, Geosci. Model Dev., 5, 845-868, 10.5194/gmd-5-845-2012, 2012.

Brown, H. Y., Wagman, B., Bull, D., Peterson, K., Hillman, B., Liu, X., Ke, Z., and Lin, L.: Validating a microphysical prognostic stratospheric aerosol implementation in E3SMv2 using observations after the Mount Pinatubo eruption, Geosci. Model Dev., 17, 5087-5121, 10.5194/gmd-17-5087-2024, 2024.

Carn, S.: Multi-Satellite Volcanic Sulfur Dioxide L4 Long-Term Global Database V4 [dataset], 10.5067/MEASURES/SO2/DATA405, 2022.

Crutzen, P. J.: Albedo enhancement by stratospheric sulfur injections: a contribution to resolve a policy dilemma?, Climatic change, 77, 211, 2006.

Deshler, T.: A review of global stratospheric aerosol: Measurements, importance, life cycle, and local stratospheric aerosol, Atmospheric Research, 90, 223-232, 2008.

Deshler, T., Johnson, B. J., and Rozier, W. R.: Balloonborne measurements of Pinatubo aerosol during 1991 and 1992 at 41 N: Vertical profiles, size distribution, and volatility, Geophysical Research Letters, 20, 1435-1438, 1993.

Deshler, T., Hervig, M., Hofmann, D., Rosen, J., and Liley, J.: Thirty years of in situ stratospheric aerosol size distribution measurements from Laramie, Wyoming (41 N), using balloon-borne instruments, Journal of Geophysical Research: Atmospheres, 108, 2003.

Dhomse, S. S., Chipperfield, M. P., Feng, W., Hossaini, R., Mann, G. W., and Santee, M. L.: Revisiting the hemispheric asymmetry in midlatitude ozone changes following the Mount Pinatubo eruption: A 3-D model study, Geophysical Research Letters, 42, 3038-3047, https://doi.org/10.1002/2015GL063052, 2015.

Emmons, L. K., Walters, S., Hess, P. G., Lamarque, J.-F., Pfister, G. G., Fillmore, D., Granier, C., Guenther, A., Kinnison, D., and Laepple, T.: Description and evaluation of the Model for Ozone and Related chemical Tracers, version 4 (MOZART-4), Geoscientific Model Development, 3, 43-67, 2010.

Gao, C. Y., Naik, V., Horowitz, L. W., Ginoux, P., Paulot, F., Dunne, J., Mills, M., Aquila, V., and Colarco, P.: Volcanic drivers of stratospheric sulfur in GFDL ESM4, Journal of Advances in Modeling Earth Systems, 15, e2022MS003532, 2023.

Golaz, J. C., Van Roekel, L. P., Zheng, X., Roberts, A. F., Wolfe, J. D., Lin, W., Bradley, A. M., Tang, Q., Maltrud, M. E., and Forsyth, R. M.: The DOE E3SM Model Version 2: Overview of the physical model and initial model evaluation, Journal of Advances in Modeling Earth Systems, 14, e2022MS003156, 2022.

Kleinschmitt, C., Boucher, O., and Platt, U.: Sensitivity of the radiative forcing by stratospheric sulfur geoengineering to the amount and strategy of the SO2injection studied with the LMDZ-S3A model, Atmos. Chem. Phys., 18, 2769-2786, 10.5194/acp-18-2769-2018, 2018.

Kleinschmitt, C., Boucher, O., Bekki, S., Lott, F., and Platt, U.: The Sectional Stratospheric Sulfate Aerosol module (S3A-v1) within the LMDZ general circulation model: description and evaluation against stratospheric aerosol observations, Geosci. Model Dev., 10, 3359-3378, 10.5194/gmd-10-3359-2017, 2017.

Kokkola, H., Korhonen, H., Lehtinen, K. E. J., Makkonen, R., Asmi, A., Järvenoja, S., Anttila, T., Partanen, A. I., Kulmala, M., Järvinen, H., Laaksonen, A., and Kerminen, V. M.: SALSA – a Sectional Aerosol module for Large Scale Applications, Atmos. Chem. Phys., 8, 2469-2483, 10.5194/acp-8-2469-2008, 2008.

Kremser, S., Thomason, L. W., von Hobe, M., Hermann, M., Deshler, T., Timmreck, C., Toohey, M., Stenke, A., Schwarz, J. P., and Weigel, R.: Stratospheric aerosol—Observations, processes, and impact on climate, Reviews of Geophysics, 54, 278-335, 2016.

Laakso, A., Korhonen, H., Romakkaniemi, S., and Kokkola, H.: Radiative and climate effects of stratospheric sulfur geoengineering using seasonally varying injection areas, Atmos. Chem. Phys., 17, 6957-6974, 10.5194/acp-17-6957-2017, 2017.

Laakso, A., Niemeier, U., Visioni, D., Tilmes, S., and Kokkola, H.: Dependency of the impacts of geoengineering on the stratospheric sulfur injection strategy–Part 1: Intercomparison of modal and sectional aerosol modules, Atmospheric Chemistry and Physics, 22, 93-118, 2022.

Liu, X.: Aerosols and Climate Effects, in: Fast Processes in Large-Scale Atmospheric Models, Wiley, 53-86, https://doi.org/10.1002/9781119529019.ch3, 2023.

Liu, X., Ma, P.-L., Wang, H., Tilmes, S., Singh, B., Easter, R., Ghan, S., and Rasch, P.: Description and evaluation of a new four-mode version of the Modal Aerosol Module (MAM4) within version 5.3 of the Community Atmosphere Model, Geoscientific Model Development, 9, 505-522, 2016.

Mills, M. J., Richter, J. H., Tilmes, S., Kravitz, B., MacMartin, D. G., Glanville, A. A., Tribbia, J. J., Lamarque, J. F., Vitt, F., and Schmidt, A.: Radiative and chemical response to interactive stratospheric sulfate aerosols in fully coupled CESM1 (WACCM), Journal of Geophysical Research: Atmospheres, 122, 13,061-013,078, 2017.

Mills, M. J., Schmidt, A., Easter, R., Solomon, S., Kinnison, D. E., Ghan, S. J., Neely III, R. R., Marsh, D. R., Conley, A., and Bardeen, C. G.: Global volcanic aerosol properties derived from emissions, 1990–2014, using CESM1 (WACCM), Journal of Geophysical Research: Atmospheres, 121, 2332-2348, 2016.

Neely III, R. R. S., A.: VolcanEESM: Global volcanic sulphur dioxide (SO2) emissions database from 1850 to present - Version 1.0 [dataset], 10.5285/76ebdc0b-0eed-4f70-b89e-55e606bcd568, 2016.

Parker, D., Wilson, H., Jones, P. D., Christy, J., and Folland, C. K.: The impact of Mount Pinatubo on world-wide temperatures, International Journal of Climatology: A Journal of the Royal Meteorological Society, 16, 487-497, 1996.

Peng, Y., Yu, P., Portmann, R. W., Rosenlof, K. H., Zhang, J., Liu, C.-C., Li, J., and Tian, W.: Perturbation of Tropical Stratospheric Ozone Through Homogeneous and Heterogeneous Chemistry Due To Pinatubo, Geophysical Research Letters, 50, e2023GL103773, https://doi.org/10.1029/2023GL103773, 2023.

Quaglia, I., Timmreck, C., Niemeier, U., Visioni, D., Pitari, G., Brodowsky, C., Brühl, C., Dhomse, S. S., Franke, H., and Laakso, A.: Interactive stratospheric aerosol models' response to different amounts and altitudes of SO 2 injection during the 1991 Pinatubo eruption, Atmospheric Chemistry and Physics, 23, 921-948, 2023.

Robock, A.: Volcanic eruptions and climate, Reviews of geophysics, 38, 191-219, 2000.

Russell, P. B., Livingston, J. M., Pueschel, R. F., Bauman, J. J., Pollack, J. B., Brooks, S. L., Hamill, P., Thomason, L. W., Stowe, L. L., Deshler, T., Dutton, E. G., and Bergstrom, R. W.: Global to microscale evolution of the

Pinatubo volcanic aerosol derived from diverse measurements and analyses, Journal of Geophysical Research: Atmospheres, 101, 18745-18763, https://doi.org/10.1029/96JD01162, 1996.

Seinfeld, J. H. and Pandis, S. N.: Atmospheric Chemistry and Physics: From Air Pollution to Climate Change, Wiley2016.

Sheng, J. X., Weisenstein, D. K., Luo, B. P., Rozanov, E., Stenke, A., Anet, J., Bingemer, H., and Peter, T.: Global atmospheric sulfur budget under volcanically quiescent conditions: Aerosol-chemistry-climate model predictions and validation, Journal of Geophysical Research: Atmospheres, 120, 256-276, 2015.

Tilmes, S., Richter, J. H., Mills, M. J., Kravitz, B., MacMartin, D. G., Vitt, F., Tribbia, J. J., and Lamarque, J. F.: Sensitivity of aerosol distribution and climate response to stratospheric SO2 injection locations, Journal of Geophysical Research: Atmospheres, 122, 12,591-512,615, 2017.

Tilmes, S., Visioni, D., Jones, A., Haywood, J., Séférian, R., Nabat, P., Boucher, O., Bednarz, E. M., and Niemeier, U.: Stratospheric ozone response to sulfate aerosol and solar dimming climate interventions based on the G6 Geoengineering Model Intercomparison Project (GeoMIP) simulations, 2022.

Vattioni, S., Weisenstein, D., Keith, D., Feinberg, A., Peter, T., and Stenke, A.: Exploring accumulation-mode H 2 SO 4 versus SO 2 stratospheric sulfate geoengineering in a sectional aerosol–chemistry–climate model, Atmospheric Chemistry and Physics, 19, 4877-4897, 2019.

Visioni, D., Bednarz, E. M., Lee, W. R., Kravitz, B., Jones, A., Haywood, J. M., and MacMartin, D. G.: Climate response to off-equatorial stratospheric sulfur injections in three Earth system models–Part 1: Experimental protocols and surface changes, Atmospheric Chemistry and Physics, 23, 663-685, 2023.

Visioni, D., MacMartin, D. G., Kravitz, B., Tilmes, S., Mills, M. J., Richter, J. H., and Boudreau, M. P.: Seasonal injection strategies for stratospheric aerosol geoengineering, Geophysical Research Letters, 46, 7790-7799, 2019.

Wang, H., Easter, R. C., Zhang, R., Ma, P. L., Singh, B., Zhang, K., Ganguly, D., Rasch, P. J., Burrows, S. M., and Ghan, S. J.: Aerosols in the E3SM Version 1: New developments and their impacts on radiative forcing, Journal of Advances in Modeling Earth Systems, 12, e2019MS001851, 2020.

Wu, M., Wang, H., Easter, R. C., Lu, Z., Liu, X., Singh, B., Ma, P.-L., Tang, Q., Zaveri, R. A., Ke, Z., Zhang, R., Emmons, L. K., Tilmes, S., Dibb, J. E., Zheng, X., Xie, S., and Leung, L. R.: Development and Evaluation of E3SM-MOSAIC: Spatial Distributions and Radiative Effects of Nitrate Aerosol, Journal of Advances in Modeling Earth Systems, 14, e2022MS003157, https://doi.org/10.1029/2022MS003157, 2022.

Yang, F. and Schlesinger, M. E.: On the surface and atmospheric temperature changes following the 1991 Pinatubo volcanic eruption: A GCM study, Journal of Geophysical Research: Atmospheres, 107, ACL 8-1-ACL 8-14, 2002.

Zhao, X. a. N. C. P.: NOAA Climate Data Record (CDR) of AVHRR Daily and Monthly Aerosol Optical Thickness (AOT) over Global Oceans (Monthly subset) (4.0) [dataset], 10.25921/w3zj-4y48, 2022.

Zhuo, Z., Kirchner, I., Pfahl, S., and Cubasch, U.: Climate impact of volcanic eruptions: the sensitivity to eruption season and latitude in MPI-ESM ensemble experiments, Atmospheric Chemistry and Physics, 21, 13425-13442, 2021.

Brown, H. Y., Wagman, B., Bull, D., Peterson, K., Hillman, B., Liu, X., Ke, Z., and Lin, L.: Validating a microphysical prognostic stratospheric aerosol implementation in E3SMv2 using observations after the Mount Pinatubo eruption, Geosci. Model Dev., 17, 5087-5121, 10.5194/gmd-17-5087-2024, 2024.

Gao, C. Y., Naik, V., Horowitz, L. W., Ginoux, P., Paulot, F., Dunne, J., Mills, M., Aquila, V., and Colarco, P.: Volcanic Drivers of Stratospheric Sulfur in GFDL ESM4, Journal of Advances in Modeling Earth Systems, 15, e2022MS003532, https://doi.org/10.1029/2022MS003532, 2023.

Hansen, J., Sato, M., Ruedy, R., Nazarenko, L., Lacis, A., Schmidt, G. A., Russell, G., Aleinov, I., Bauer, M., Bauer, S., Bell, N., Cairns, B., Canuto, V., Chandler, M., Cheng, Y., Del Genio, A., Faluvegi, G., Fleming, E., Friend, A., Hall, T., Jackman, C., Kelley, M., Kiang, N., Koch, D., Lean, J., Lerner, J., Lo, K., Menon, S., Miller, R., Minnis, P., Novakov, T., Oinas, V., Perlwitz, J., Perlwitz, J., Rind, D., Romanou, A., Shindell, D., Stone, P., Sun, S., Tausnev, N., Thresher, D., Wielicki, B., Wong, T., Yao, M., and Zhang, S.: Efficacy of climate forcings, Journal of Geophysical Research: Atmospheres, 110, https://doi.org/10.1029/2005JD005776, 2005.

Marshall, L., Johnson, J. S., Mann, G. W., Lee, L., Dhomse, S. S., Regayre, L., Yoshioka, M., Carslaw, K. S., and Schmidt, A.: Exploring How Eruption Source Parameters Affect Volcanic Radiative Forcing Using Statistical Emulation, Journal of Geophysical Research: Atmospheres, 124, 964-985, https://doi.org/10.1029/2018JD028675, 2019.

Mills, M. J., Schmidt, A., Easter, R., Solomon, S., Kinnison, D. E., Ghan, S. J., Neely III, R. R., Marsh, D. R., Conley, A., and Bardeen, C. G.: Global volcanic aerosol properties derived from emissions, 1990–2014, using CESM1 (WACCM), Journal of Geophysical Research: Atmospheres, 121, 2332-2348, 2016.

Toohey, M., Krüger, K., Schmidt, H., Timmreck, C., Sigl, M., Stoffel, M., and Wilson, R.: Disproportionately strong climate forcing from extratropical explosive volcanic eruptions, Nature Geoscience, 12, 100-107, 10.1038/s41561-018-0286-2, 2019.

Zhuo, Z., Fuglestvedt, H. F., Toohey, M., and Krüger, K.: Initial atmospheric conditions control transport of volcanic volatiles, forcing and impacts, Atmos. Chem. Phys., 24, 6233-6249, 10.5194/acp-24-6233-2024, 2024.